Environmental Science Processes & Impacts

Hg isotopes reveal in-stream processing and legacy inputs in East Fork Poplar Creek, Oak Ridge, Tennessee, USA

Journal:	*Environmental Science: Processes & Impacts*
Manuscript ID	EM-ART-11-2017-000538.R1
Article Type:	Paper
Date Submitted by the Author:	27-Feb-2018

Complete List of Authors:	Demers, Jason; University of Michigan, Department of Earth and Environmental Sciences Blum, Joel; University of Michigan, Department of Earth and Environmental Sciences Brooks, Scott; Oak Ridge National Laboratory, Environmental Sciences Division Donovan, Patirck; University of Michigan, Department of Earth and Environmental Sciences Riscassi, Ami; University of Virginia, Environmental Sciences Miller, Carrie; Troy University, Department of Biology Zheng, Wang; Arizona State University, School of Earth and Space Exploration Gu, Baohua; Oak Ridge National Laboratory, Environmental Sciences Division

SCHOLARONE™
Manuscripts

Hg isotopes reveal in-stream processing and legacy inputs in East Fork Poplar Creek, Oak Ridge, Tennessee, USA

[1*]Jason D. Demers, [1]Joel D. Blum, [2]Scott C. Brooks, [1]Patrick M. Donovan, [2,3]Ami L. Riscassi, [2,4]Carrie L. Miller, , [2,5]Wang Zheng, and [2]Baohua Gu

[1]Department of Earth and Environmental Sciences, University of Michigan, Ann Arbor, MI 48109, USA
[2]Environmental Sciences Division, Oak Ridge National Laboratory, Oak Ridge, TN 37831, USA
[3]Present address: Department of Environmental Sciences, University of Virginia, Charlottesville, VA 22904-4123, USA
[4]Present address: Department of Biology, Troy University, Troy, AL 36082, USA
[5]Present address: School of Earth and Space Exploration, Arizona State University, Tempe, AZ 85287, USA

*Corresponding author: J. D. Demers, Department of Earth and Environmental Sciences, University of Michigan, 1100 N. University Ave., Ann Arbor, MI 48109, USA (jdemers@umich.edu)

Environmental Significance Statement

It is challenging to identify, track, and assess the *in situ* processing of Hg sources that contribute to ongoing Hg loading and bioaccumulation within aquatic ecosystems. As controls on Hg emissions to the atmosphere and industrial releases to surface waters continue to reduce inputs of new Hg to aquatic ecosystems, it becomes increasingly important to understand how legacy Hg accumulated in soils and sediment may delay recovery. Mercury stable isotope measurements suggested that legacy mercury, generally thought to reside in recalcitrant forms, likely contributes to increases in Hg flux along the flow path of a point-source-impacted headwater stream. By linking Hg isotopes and hydrology, this study provides a framework that integrates stable Hg isotope techniques with more traditional stream- and watershed-scale approaches.

Hg isotopes reveal in-stream processing and legacy inputs in East Fork Poplar Creek, Oak Ridge, Tennessee, USA

[1*]Jason D. Demers, [1]Joel D. Blum, [2]Scott C. Brooks, [1]Patrick M. Donovan, [2,3]Ami L. Riscassi, [2,4]Carrie L. Miller, [2,5]Wang Zheng, and [2]Baohua Gu

[1]Department of Earth and Environmental Sciences, University of Michigan, Ann Arbor, MI 48109, USA
[2]Environmental Sciences Division, Oak Ridge National Laboratory, Oak Ridge, TN 37831, USA
[3]Present address: Department of Environmental Sciences, University of Virginia, Charlottesville, VA 22904-4123, USA
[4]Present address: Department of Biology, Troy University, Troy, AL 36082, USA
[5]Present address: School of Earth and Space Exploration, Arizona State University, Tempe, AZ 85287, USA

*Corresponding author: J. D. Demers, Department of Earth and Environmental Sciences, University of Michigan, 1100 N. University Ave., Ann Arbor, MI 48109, USA (jdemers@umich.edu)

Abstract:

Natural abundance stable Hg isotope measurements were used to place new constraints on sources, transport, and transformations of Hg along the flow path of East Fork Poplar Creek (EFPC), a point-source contaminated headwater stream in Oak Ridge, Tennessee. Particulate-bound Hg in the water column of EFPC within the Y12 National Security Complex, was isotopically similar to average metallic Hg(0) used in industry, having a mean δ^{202}Hg value of -0.42 ± 0.09‰ (1SD) and near-zero Δ^{199}Hg. On average, particulate fraction δ^{202}Hg values increased downstream by 0.53‰, while Δ^{199}Hg decreased by -0.10‰, converging with the Hg isotopic composition of the fine fraction of streambed sediment along the 26 km flow path. The dissolved fraction behaved differently. Although initial Δ^{199}Hg values of the dissolved fraction were also near-zero, these values increased transiently along the flow path. Initial δ^{202}Hg values of the dissolved fraction were more variable than in the particulate fraction, ranging from -0.44 to 0.18‰ among three seasonal sampling campaigns, but converged to an average δ^{202}Hg value of 0.01 ±0.10‰ (1SD) downstream. Dissolved Hg in the hyporheic and riparian pore water had higher and lower δ^{202}Hg values, respectively, compared to dissolved Hg in stream water. Variations in Hg isotopic composition of the dissolved and suspended fractions along the flow path suggest that: (1) physical processes such as dilution and sedimentation do not fully explain decreases in total mercury concentrations along the flow path; (2) in-stream processes include photochemical reduction, but microbial reduction is likely more dominant; and (3) additional sources of dissolved mercury inputs to EFPC at baseflow during this study predominantly arise from the hyporheic zone.

Environmental Significance Statement

It is challenging to identify, track, and assess the *in situ* processing of Hg sources that contribute to ongoing Hg loading and bioaccumulation within aquatic ecosystems. As controls on Hg emissions to the atmosphere and industrial releases to surface waters continue to reduce inputs of new Hg to aquatic ecosystems, it becomes increasingly important to understand how legacy Hg accumulated in soils and sediment may delay recovery. Mercury stable isotope measurements suggested that legacy mercury, generally thought to reside in recalcitrant forms, likely contributes to increases in Hg flux along the flow path of a point-source-impacted headwater stream. By linking Hg isotopes and hydrology, this study provides a framework that integrates stable Hg isotope techniques with more traditional stream- and watershed-scale approaches.

1. Introduction

Understanding how aquatic ecosystems contaminated with mercury (Hg) will recover as atmospheric emissions and industrial point source discharges are controlled has become an important area of Hg research. Key to predicting recovery from Hg contamination is understanding the mobilization of legacy Hg sources and the subsequent bioavailability and biogeochemical cycling of mobilized Hg within aquatic ecosystems. Over the last two decades, observational and mass balance studies, *in situ* field manipulations, and isotope spike experiments have all provided valuable insight into Hg mobilization, bioavailability, and biogeochemical cycling.[1-11] Nonetheless, discerning the importance of potential sources and evaluating *in situ* processes that influence legacy Hg dynamics in complex ecosystems has remained challenging.

Herein, we take a multi-seasonal hydro-biogeochemical flow path approach that utilizes natural abundance stable Hg isotope ratio measurements to place new constraints on sources, transport, and *in-situ* transformations of Hg in East Fork Poplar Creek (EFPC), Oak Ridge, Tennessee. We document variations in Hg isotopic composition in stream water dissolved and particulate phases, hyporheic zone pore water and sediment, riparian floodplain pore water and sediment, streambed periphyton, and streambed sediment in EFPC, and interpret the evolution of isotopic signatures along the flow path in terms of experimentally derived fractionation patterns associated with biogeochemical processes[12, 13] and with regard to the addition of Hg from riparian floodplains and the hyporheic zone.

The East Fork Poplar Creek ecosystem is heavily contaminated with Hg from operations to separate ^{6}Li isotopes for thermonuclear weapons development during the 1950's and early 1960's at the Y-12 National Security Complex (Y12), Oak Ridge, TN.[14] During that time, an estimated 193,000 +/- 27,000 kg of metallic Hg was lost to the local soil and groundwater environment, and 128,000 +/- 35,000 kg of particulate-bound and dissolved Hg(II) associated with neutralized nitric acid waste was discharged directly to EFPC from the storm drain system underlying Y12.[14] These historical releases of Hg have resulted in a legacy of Hg contamination in streambed sediment, streambanks, and floodplain soils downstream of the Y12 complex.[15, 16]

The largest known remaining sources of inorganic Hg to Upper EFPC (i.e., within the Y12 boundary) include dissolved Hg(II) species discharged from the storm drain network underlying the Y12 facility (~ 60% +/- 10%), dissolved Hg(0) from metallic mercury within streambed sediments along the first 300 m of Upper EFPC (~15% +/- 5%), and a small amount of post-remedial-action dissolved Hg(0) emanating from a groundwater spring near the Y12 boundary (~3.5%)[14]. Inputs of dissolved Hg(0) to the creek are either lost by volatilization[17-20] or are oxidized. Dissolved Hg(II) species become largely associated with naturally occurring dissolved and particulate organic matter.[21-23] Despite the successes of remedial strategies within the Y12 complex, discharges of total dissolved and particulate-bound Hg at the Y12 boundary continued to be ~10 g/d (~ 330 ng/L) under managed baseflow conditions maintained from 1997 to 2014.[14, 24]

The inventory of Hg in the EFPC ecosystem and the transport of dissolved and particulate Hg under both baseflow and stormflow conditions have been studied. *Southworth et al.*[15, 16] and *Riscassi et al.*[25] similarly concluded that particulate-bound Hg associated with streambed sediment, streambed biofilm, and streambank soils within Lower EFPC (downstream of the Y12 boundary) was primarily responsible for the large increases in Hg export during wet weather high-flow conditions. *Riscassi et al.*[25] further suggested that total dissolved mercury (THg_d) associated with dissolved organic matter (DOM) was transported to the stream predominantly from watershed soils (rather than from upstream point sources) during high flow events.

Under baseflow conditions, in contrast, *Southworth et al.*[15, 16] concluded that ongoing inorganic Hg inputs from the Y12 complex into Upper EFPC (upstream of the Y12 boundary) continue to sustain waterborne Hg concentrations throughout EFPC. However, *Riscassi et al.*[25] determined that ~60% of annual baseflow hydrologic discharge in the lower reaches of EFPC was derived from diffuse groundwater. Although the THg_d load contributed by these diffuse inputs could not be evaluated, they represent a potential source of legacy Hg to the stream channel. Mercury in soils and sediment resides in highly insoluble forms[16, 26-29] that are generally thought to have little impact on total dissolved mercury (THg_d) concentrations;[15] however, recent experiments with EFPC floodplain soils suggest that a small portion of these recalcitrant legacy Hg reservoirs may be re-mobilized.[25, 30]

Waterborne concentrations of THg_d and particulate-bound mercury (THg_p) decrease with distance downstream from Y12 during baseflow in EFPC.[14, 31] Dilution with low Hg concentration waters from non-Y12-contaminated tributaries and groundwater likely contribute to these decreases in THg concentrations.[25, 32, 33] However, *Southworth et al.*[15] noted that THg fluxes (not just concentrations) also decreased downstream under baseflow conditions, suggesting THg removal from the water column by sedimentation of the particulate phase and accumulation in biofilm coatings on the streambed. In contrast, waterborne concentrations of MeHg increase with distance downstream of Y12,[14, 31] resulting in a decoupling of inorganic Hg and MeHg concentrations along the flow path. *Riscassi et al.*[25] observed that the highest concentrations of methylmercury (MeHg) in downstream surface waters occurred during baseflow, implying a significant role for in-stream (and, perhaps, near-stream) processes within the streambed hyporheic zone and streambed periphyton.

The overarching objective of this study was to utilize Hg isotopes to further elucidate the in-stream processes and source input(s) that influence waterborne mercury dynamics along the flow path of EFPC, a mercury contaminated headwater stream. Specifically, we sought to understand whether in-stream processes, such as photochemical and microbial reduction, in conjunction with physical processes, such as sedimentation, mixing, and dilution, may influence downstream decreases in THg_p and THg_d concentrations. Additionally, we aimed to characterize the mercury isotopic composition of potential legacy sources of THg_d to stream water (e.g., inputs from the hyporheic zone and riparian floodplains) downstream of the Y12 complex, and to assess their role in sustaining baseflow THg_d concentrations along the flow path of EFPC.

2. Methods

2.1. Site Description

The headwaters of East Fork Poplar Creek (EFPC) originate within the US Department of Energy (DOE) Y-12 National Security Complex (Y12), and flow 26 km downstream to its confluence with Poplar Creek (Figure 1).[24] Locations along EFPC are denoted by their distance upstream from this confluence, in kilometers. Upon construction of Y12, headwater tributaries were confined within a buried storm drain network[14] that discharges into an open industrial ditch, flowing about 3 km downstream to the Y12 boundary at Station 17 (EFK23.4). This channelized reach of EFPC within the Y12 boundary is administratively referred to as Upper EFPC. Beginning in August 1996, flow in Upper EFPC was augmented with the addition of water piped from the Clinch River in order to maintain a minimum flow of ~300 l/s at Station 17,[24] thereby reducing the mercury concentration of waters exported from Y12 to ~300 ng/L.[15] This managed flow regime was maintained throughout the period of our study, but was terminated in April 2014. Beginning at the Y12 boundary, Lower EFPC is more naturally meandering as it passes through the city of Oak Ridge for about 15 km, and then across more forested Oak Ridge Reservation land. The large amount of impervious surface within Y12 and the city of Oak Ridge results in rapid storm water runoff, flashy flows, and shifting loads of streambed sediment. The streambed consists of a mixture of coarse gravel, cobble, and bedrock outcrops, about half of which is typically covered by silt, sand, and small gravel.[24] The surface of the streambed is typically covered with biofilm coatings that are rapidly replaced following high flow scouring events. The stream corridor throughout Lower EFPC is mostly forested, with narrow riparian floodplains increasing in their extent further downstream (National Wetlands Inventory). These riparian wetland floodplains are classified as palustrine forested broad-leaved deciduous and temporarily flooded (PFO1A; www.fws.gov/wetlands/data/mapper.html). Approximately 2 km^2 of these riparian floodplains downstream of Y12 have Hg-contaminated soils.[15] Total watershed area of EFPC is 76.9 km^2. Three small tributaries with drainage areas ranging from 5.6 to 6.6 km^2 enter EFPC at EFK20, EFK16, and EFK10.[34] The city of Oak Ridge wastewater treatment facility (ORWTF) discharges to EFPC at EFK13.5. A more detailed description of the EFPC watershed is available elsewhere.[14, 15, 24] The regional reference site for this study is located ~25 km northeast of Y12, has no known point-sources of Hg contamination, and is characterized by typical background levels of mercury in water and sediment (Hinds Creek, HCK10; 36.1411ºN, 84.0508ºW; see Figure 1 in *Donovan et al.*[34]).

2.2. Study Design and Sample Collection

We employed both synoptic and intensive site sampling strategies during three seasonal sampling campaigns (October 2011, April 2012, and August 2012). All samples were collected during baseflow conditions (Figure S1). Synoptic sampling consisted of eight stream sampling locations along the flow path of EFPC, ranging from EFK5.0 to EFK25.4, two of which were within the Y12 boundary along Upper EFPC (Figure 1). Synoptic samples were collected to assess changes in the isotopic composition of waterborne mercury along the flow path of EFPC.

Water samples for analysis of total dissolved mercury (THg_d) were immediately filtered in the field (0.45 µm cellulose nitrate sterile analytical filter units; Thermo Scientific Nalgene #130-4045), poured into Teflon bottles, and preserved to 0.5% (v/v) Trace Metal Grade (TMG) HCl. Filters were retained for analysis of total particulate-bound mercury (THg_p). Both filtered and unfiltered stream water was also collected for analysis of methylmercury (MeHg); these samples were stored in polycarbonate bottles and preserved to 0.5% (v/v) with TMG HCl. All bottles for THg and MeHg were trace metal cleaned and blank-checked prior to use. Dissolved organic carbon (DOC) samples were syringe filtered (0.45 µm Supor) onsite into 40 ml amber I-Chem vials; anion (NO_3^-, SO_4^{2-}, Cl^-) samples were syringe filtered (0.45 µm polypropylene) onsite into 60 ml HDPE bottles, following methods of *Demers et al.* [35]. All samples were put into coolers with ice in the field and refrigerated at 4ºC upon return to the lab at the end of each day.

During the April and August sampling campaigns, bulk stream water samples were also collected from three synoptic sampling sites (EFK25.4, EFK22.3, and EFK5.0) for separation and analysis of dissolved gaseous mercury (DGM). Concentrations of stream water DGM along the flow path were low, and therefore DGM samples were not analyzed for Hg isotopic composition.

Intensive site sampling was completed during each season at two sites along EFPC (EFK5.0, EFK22.3) and at a regional reference stream, Hinds Creek (HCK10), located ~25 km northeast of Y12 (Figure 1). These intensive sampling efforts were designed to assess differences in mercury isotopic composition within various components of the stream ecosystem. At each intensive site, we collected surface water, hyporheic pore water from both the center and side of the main channel, and streambed biofilm coatings. At EFK22.3, we also collected surface water and pore water from a Hg-contaminated riparian floodplain. Pore water samples were collected with a Henry sampler (i.e., a temporary piezometer, www.mheproducts.com). Biofilm was scrubbed off the surface of 10-20 rocks in each of the study reaches, and the resulting slurry was transferred to a trace metal clean polycarbonate bottle, stored on ice in the field, and placed in refrigeration upon return to the lab at the end of each day. Similar to synoptic sampling, intensive site surface water and pore water samples were collected for analysis of THg_d, THg_p, filtered MeHg, unfiltered MeHg, DOC, Specific UV Absorbance ($SUVA_{254}$), anions, and pH.

2.3. Hydrologic Discharge and Mercury Fluxes

Gauging stations were located at the Y12 boundary (Station 17, EFK23.4) and downstream near EFK5.0. The gauging station at EFK23.4 (formerly, United States Geological Survey (USGS) #03538235) is currently operated by Y12, consists of a water-stage recorder and a concrete weir, and has been continuously maintained since it was established in 1992[36]. Hourly mean discharge (m^3/s) at this gauging station was provided courtesy of K. Hanzelka and was calculated from a stage-discharge rating curve established by the USGS. The gauging station at EFK5.4 was located at a previously established USGS surface water monitoring site (USGS ID# 03538250) which had a period of record from 1960 through 1988[37], and was re-established in

2011 by *Riscassi et al.*[25] Hourly mean discharge (m^3/s) at this gauging station was based on stage readings at 6 minute intervals measured by a pressure transducer within a stilling well. Daily mean discharge (m^3/s) data for the City of Oak Ridge wastewater treatment facility (ORWTF) were provided courtesy of J. Sproles. Water levels at EFK23.4 and the ORWTF were measured during all sampling periods; water levels at EFK5.4 were recorded beginning in February 2012. Therefore, October 2012 baseflow discharge and concentration data were used to represent October 2011 baseflow conditions for estimates of flux. Herein, we take the conservative approach of applying a discharge uncertainty based on a USGS rating system indicating that 95% of daily discharges at these stations are within 10% of the true value;[36, 37] this uncertainty estimate includes both qualitative and quantitative factors and is believed to be > 1SD.

Whereas hydrologic discharge (Q) at EFK23.4, EFK5.4, and ORWTF were measured directly, we estimated the discharge from tributaries and diffuse sources (combined) by difference: $(Q_{Tributaries} + Q_{Diffuse}) = (Q_{EFK5.4}) - (Q_{EFK23.4}) - (Q_{ORWTF})$. Instantaneous mercury flux (Φ) at EFK23.4, EFK5.0 and ORWTF was calculated by multiplying discharge (Q) by concentration (C). Uncertainty in concentration measurements was based on the average relative standard deviation (RSD) of replicate stream water samples taken from upstream and downstream sites along EFPC (8.4% RSD, n = 5; see section 2.4). We calculated maximum potential tributary mercury flux by multiplying $(Q_{Tributaries} + Q_{Diffuse})$ by the average concentration of tributaries; thus, some portion of the estimated tributary flux is likely attributable to diffuse sources and this is considered in the discussion. Finally, we estimated the minimum diffuse mercury flux ($\Phi_{Diffuse}$) by subtraction: $(\Phi_{Diffuse}) = (\Phi_{EFK5.0}) - (\Phi_{EFK23.4}) - (\Phi_{ORWTF}) - (\Phi_{Tributaries})$. For discharge and flux calculations, uncertainties for sums and differences, and relative uncertainties for products, were propagated in quadrature.[38]

2.4. Concentration Analysis

Total Hg and MeHg concentrations were measured using standard methods and samples were analyzed in batches with quality control that included independent primary and secondary standards, continuing calibration verification standards, continuing calibration blanks, matrix spike recovery tests, analysis of duplicate field samples, reference materials, and equipment and procedural blanks. Upon return to the lab, field-acidified THg_d surface water samples were oxidized to 1% BrCl by volume (verified to be Hg-free) and allowed to react in the dark at 4ºC for one month prior to analysis. Stream water and pore water THg_d concentrations were measured according to EPA Method 1631[39] using an automated cold-vapor atomic fluorescence spectrometer (CVAFS; RA-3F, Nippon Instruments). Particulate-bound mercury (THg_p) retained on filters was combusted offline and the released mercury was trapped in an oxidizing solution that was then measured for THg concentration according to EPA Method 1631 using a cold-vapor atomic absorption spectrometer (CVAAS; MA-2000, Nippon Instruments; see section 2.5.1), and scaled to the volume of filtered stream water. Biofilm THg samples were dewatered via centrifugation, freeze-dried, homogenized in an alumina grinding cylinder in a mixer mill, and analyzed by offline combustion, similar to filters. Filtered and unfiltered stream water

MeHg was analyzed by distillation purge and trap according to EPA Method 1630[40] using dual isotope spike dilution.[41]

Dissolved gaseous mercury (DGM) was extracted from stream water in the laboratory, within one hour of collection. In the field, a 2L Pyrex media bottle was filled with 1L of stream water with minimal agitation, capped, double bagged, wrapped in black plastic, and immediately put in a cooler on ice. These stream water samples were immediately returned to the lab for DGM extraction by purge and trap using similar methods as for filtered stream water sample preparation for mercury isotope analysis (see section: 2.5.2), with several important differences. First, bulk stream water was unaltered prior to purging of DGM (i.e., the sample was not filtered, acidified, oxidized, or reduced). Second, the cap of the sample collection bottle was fitted with two-way valves that allowed connection to the purge and trap system without losing DGM volatilized to the headspace during transport. Third, testing showed that samples could be completely purged within 90 minutes. Purged DGM was oxidized in 1% $KMnO_4$ (mass/mass) in 10% sulfuric acid (v/v) (hereafter referred to as 1% $KMnO_4$) that was measured for THg concentration according to EPA Method 1631[39] via CVAAS and scaled to volume of sampled stream water.

DOC was analyzed using high-temperature platinum-catalyzed combustion followed by infrared detection of CO_2 (Shimazdu TOC-L). UV absorbance data was collected with a Hewlett-Packard 8453 spectrophotometer using a 1.0 cm path length and ultrapure water as a blank. Specific ultraviolet absorbance ($SUVA_{254}$) values were determined by dividing UV absorbance at 254 nm (1/m) by DOC concentration (mg/L) and is reported in units of liters per milligram carbon per meter (L/mg C m)[42]. Inorganic anions were analyzed by a Dionex DX-500 ion chromatograph equipped with a Dionex AS15 analytical column and a Dionex EG40 eluent generator. MeHg, DOC, UV absorbance, and inorganic anion analyses were completed in the Environmental Sciences Division (ESD) at Oak Ridge National Laboratory (ORNL), as previously described.[21, 43, 44] All other measurements were completed in the Biogeochemistry and Environmental Isotope Geochemistry Laboratory at the University of Michigan.

2.5. Sample Preparation for Isotope Analysis

2.5.1. Offline Combustion of Filters and Biofilm. Biofilm and THg_p retained on filters were prepared by two-stage combustion with inline trapping of released Hg in order to remove matrix interferences and concentrate Hg for isotopic analysis, following methods detailed in *Demers et al.*[45] Filters were freeze-dried prior to combustion. Volatilized reduced Hg(0) was re-oxidized and trapped within a 24 g solution of 1% $KMnO_4$. To quantify THg_p released from each sample, the 1% $KMnO_4$ combustion trap solution was reduced with hydroxylamine hydrochloride, and a small aliquot was diluted with 1% BrCl for analysis by CVAAS (see section 2.4). Reduced solutions were concentrated into secondary 1% $KMnO_4$ traps to achieve required 1-5 ng/g concentration for isotopic analysis, as well as to further remove matrix interferences. The Hg concentration of a small aliquot of this transfer trap solution was

measured to determine full procedural recovery of reference materials, as well as to allow matching of standard and sample concentrations for isotope analysis.

Offline-combustion performance was monitored with procedural blanks and by percent recovery of reference materials. Average procedural blanks were 0.004 ng/g THg (± 0.002 ng/g, 1SD, n=21) prior to transfer, and 0.015 ng/g THg (± 0.003 ng/g, 1SD, n=11) subsequent to transfer, typically representing <1% of sample solutions. We combusted NIST SRM 1944 (NY/NJ Waterway Sediment; 3400 ± 500 ng/g) with recovery ranging from 94.8% to 103.9% (99.4% ± 3.1%, 1SD, n=8), and NIST SRM 1515 (Apple Leaves, 44 ± 4 ng/g) with recovery ranging from 91.2% to 94.3% (92.7% ± 1.2%, 1SD, n=5) (Table 2).

2.5.2. Purging and Trapping of Filtered Stream Water and Pore Water Samples. Mercury in filtered stream water and pore water samples was purged and trapped into 1% $KMnO_4$ solution for isotope analysis. Previously acidified and oxidized stream water samples were diluted by at least 50% with similarly acidified and oxidized Hg-free de-ionized water, and thoroughly mixed. Dilution of samples minimized potential matrix interferences, ensuring high recoveries. Diluted samples were then pre-reduced with 1000 µl of 30% hydroxylamine hydrochloride [39], capped tightly, and allowed to react for one hour. The remainder of the purge and trap procedure involving $SnCl_2$ reduction and subsequent re-oxidization and trapping of mercury within a 1% $KMnO_4$ solution followed methods detailed in *Demers et al.*[45] To quantify purge and trap recovery, Hg concentration of the 1% $KMnO_4$ trap solution was determined as outlined for the combustion trap solutions (see section 2.5.1), scaled to total solution mass, and compared to total mass of Hg in the original sample. Recovery of Hg from sample solutions was 98.9% ± 3.3% (1SD, n = 44) (Table S1, Table S2). We also monitored the performance of the purge and trap system with procedural blanks and procedural standards. Procedural blanks consisted of Hg-free de-ionized water that was acidified and oxidized the same as samples. Procedural standards consisted of either 15 ng or 35 ng of Hg (NIST SRM 3133), representing a range of sample concentrations. Standard aliquots were added to one or two 2L media bottles, and diluted to 1L with Hg-free de-ionized water that was acidified and oxidized to match the matrix of sample solutions. Procedural blanks and standards were purged, trapped, and analyzed in the same manner as samples. Final procedural blank 1% $KMnO_4$ solutions (0.013 ng/g ± 0.005 ng/g, 1SD, n=9) typically represented <1% of sample solutions. Procedural standard recovery was 97.3% (± 3.2%, 1SD, n = 14). Purge and trap procedural standards using NIST3133 were not significantly fractionated relative to NIST SRM 3133 bracketing standards (Table 2).

2.6. Mercury Isotope Analysis

Mercury isotopic composition was measured using a multiple collector inductively coupled plasma mass spectrometer (MC-ICP-MS; Nu Instruments) using continuous flow vapor generation with Sn(II) reduction.[46, 47] We employed an arrangement of faraday cups that allowed for simultaneous collection of masses 196, 198, 199, 200, 201, 202, 203, 204, 205, and 206. Analyses were run at 1-5 ng/g Hg, with standard concentrations matching sample concentrations

to within 5%. Instrumental bias was corrected using an internal standard (NIST SRM 997, $^{205}Tl/^{203}Tl$ ratio of 2.38714) and sample-standard bracketing using NIST SRM 3133 Hg standard. Isobaric interferences from ^{204}Pb were monitored to allow correction using mass 206; however, interferences were always negligible. On-peak zero corrections were applied to all masses.

We report isotopic compositions as permil (‰) deviations from the average of NIST SRM 3133 bracketing standards using delta notation:

$$\text{(Eq 1)}\quad \delta^{xxx}Hg\ (‰) = ([(^{xxx}Hg/^{198}Hg)_{unknown} / (^{xxx}Hg/^{198}Hg)_{NIST\ SRM\ 3133}] - 1) * 1000$$

where xxx is the mass of each Hg isotope between ^{199}Hg and ^{204}Hg. We use $\delta^{202}Hg$ to report mass dependent fractionation (MDF). Mass independent fractionation (MIF) is reported as the deviation of the isotope ratio from the theoretically predicted values based on the kinetic mass-dependent fractionation law and measured $\delta^{202}Hg$.[47] MIF is reported in "capital delta" notation ($\Delta^{xxx}Hg$) in units of permil (‰) (Equation 2), and is well approximated for small ranges in delta values (≤ 10 ‰) by Equation 3:

$$\text{(Eq 2)}\quad \Delta^{xxx}Hg\ (‰) = 1000 \times (\{\ln[(\delta^{xxx}Hg/1000) + 1]\} - \beta \times \{\ln[(\delta^{202}Hg/1000) + 1]\})$$

$$\text{(Eq 3)}\quad \Delta^{xxx}Hg\ (‰) \approx \delta^{xxx}Hg - (\delta^{202}Hg \times \beta)$$

where xxx is the mass of each Hg isotope 199, 200, 201, 204 and β is a constant for each isotope (0.252, 0.502. 0.752, 1.493, respectively).[47]

We characterized the uncertainty of Hg isotope measurements using a secondary standard that is widely distributed (UM-Almadén), as well as with procedural standards for each natural environmental matrix.[47] To characterize the reproducibility of the mass spectrometry, we measured the isotopic composition of UM-Almadén several times (5-7x) at representative low and high analytical concentrations within each analytical session. The 2SD uncertainty was then generated from the average of session averages for each delta value. Internal precision was typically lower than the external reproducibility of the method. For procedural standards, we calculated uncertainty as 2SE of the average of session averages. A separate estimate of procedural uncertainty was made for each sample matrix: for stream water and pore water THg_d, the procedural uncertainty was generated via purge and trap of NIST SRM 3133; for particulate-bound mercury (THg_p) retained on filters and biofilm, the procedural standard was generated by offline combustion of NIST SRM 1944 and NIST SRM 1515; all as described in section 2.5. We represent the uncertainty of samples with the uncertainty (2SE) of associated procedural standards; however, where the 2SE of procedural standards was less than the 2SD of UM-Almadén, we instead represent sample uncertainty using UM-Almadén. The uncertainty associated with the isotopic composition of UM-Almadén, procedural standards, and reference materials are presented in Table 2.

3. Results and Discussion

3.1. Stream Water Mercury Concentrations

Concentrations of mercury associated with the dissolved aqueous phase (THg_d, <0.45 µm, 11.4 to 239.8 ng/L) and suspended particulates (THg_p, >0.45 µm, 30.5 to 253.2 ng/L) decreased rapidly along the 26 km flow path from the headwaters of EFPC to its confluence with Poplar Creek (Table S3, Figure S2), consistent with previous observations.[31, 48] A limited number of measurements suggest that dissolved gaseous mercury (DGM) concentrations also decrease along the flow path (Table S3). Within the channelized Upper EFPC, DGM constituted < 10% of typical dissolved mercury concentrations at Station 8 (EFK25.4) and was rapidly oxidized and/or volatilized from the water column (Table S3). Thus, mercury transport was dominated by the oxidized phase, with 53-87% associated with particulates and 13-48% associated with the dissolved phase. Despite sharp declines along the flow path, dissolved and particulate-bound mercury concentrations remained elevated by an order of magnitude, or more, over non-Y12-impacted tributary and reference streams (background THg_d ranged from <0.05 to 0.59 ng/L; background THg_p ranged from 0.71 to 15.2 ng/L).

On a mass basis, suspended particulate THg_p concentrations also decreased from 60.3 µg/g (±26.7 µg/g, 1SD, n = 3) to 14.9 µg/g (±6.0 µg/g, 1SD, n = 3) along the flow path (Figure S2, Table S3). These decreasing THg_p concentrations mostly tracked those of the <125 µm fine-fraction of streambed sediment,[34] except in two localized reaches (EFK10, EFK18) where streambed sediment was likely influenced by elevated Hg concentrations in streambank and/or floodplain soil.[49, 50] Otherwise, streambank soil mercury concentrations and inventories are generally lower further downstream, although concentrations remain highly variable and elevated by an order of magnitude, or more, above background levels.[16, 50] Mercury concentrations in the mobile suspended particulate phase are likely integrated over longer reaches than in streambed sediments.

Bulk (< 2 mm) streambed sediment had Hg concentrations that were 8.4 to 57 µg/g lower than the co-located <125 µm fine fraction and suspended particulates, following expected concentration-grain size relationships, and did not uniformly decrease along the flow path.[34] Sampling at kilometer intervals, *Brooks et al.*[49] similarly found that sediment Hg concentrations did not decrease uniformly with distance downstream. Bulk (< 2 mm), coarse (1-2 mm), and medium (250 µm – 1 mm) size fractions decreased in Hg concentration through Upper EFPC, but remained relatively constant downstream of Y12, except for within aforementioned localized high concentration hotspots.[49] Contrary to expectations, the 125- 250 µm fraction examined by *Brooks et al.*[49] continued to decrease in Hg concentration in the lower reaches of EFPC to lower values than observed in all other size fractions.[16, 34, 49] Overall, our observations of suspended THg_p were most consistent in grain size and Hg concentration with the <125 µm fine-fraction of streambed sediment.[16, 34] Although the < 125 µm fine-fraction likely represents only a small proportion of the streambed sediment (< 10%), this and smaller size fractions typically dominate the suspended phase at baseflow.

In contrast with dissolved and particulate inorganic mercury, methylmercury (MeHg) concentrations increased downstream of Y12; $MeHg_d$ ranged from 0.05 ng/L to 0.25 ng/L, and $MeHg_p$ ranged from 0.01 to 0.15 ng/L (Figure S2, Table S3). This is also consistent with previous observations that have demonstrated a decoupling of total mercury and methylmercury dynamics along the flow path of EFPC.[31, 48] Methylmercury was predominantly associated with the dissolved phase, which accounted for 54-92% of total waterborne MeHg, with the proportion of THg_d as $MeHg_d$ (%$MeHg_d$) ranging up to only 1.8% along the flow path. Despite the high loads of inorganic mercury within the EFPC ecosystem, stream water MeHg concentrations did not exceed 0.25 ng/L. These concentrations of $MeHg_d$ in stream water were greater than $MeHg_d$ concentrations at our regional reference site (Hinds Creek, HCK10; mean = 0.04 ng/L, 1SD < 0.01 ng/L, n = 3), but are similar to some non-point-source impacted riparian wetland influenced streams studied in other regions.[4, 51-53]

3.2. Hydrologic Discharge and Mercury Fluxes

Fluxes of water and mercury along the flow path varied with season. Whereas managed stream flow at the Y12 boundary (EFK23.4) was relatively constant (0.25 ± 0.01 m^3/s, 1SD), stream flow downstream at EFK5.0 was more variable, ranging from 0.95 ± 0.10 m^3/s (1SD) in October to 1.22 ± 0.12 m^3/s (1SD) in April (Table 1). Thus, in April, prior to leaf-out and the onset of evapotranspiration, flow emanating from watershed-derived sources (not including Y12 or the ORWTF) was 45% ± 3% (1SD) greater than in August and October (Table 1). This watershed-derived component is likely dominated by tributary flow, but also includes diffuse contributions of groundwater discharging directly to the stream from the hyporheic zone and riparian wetlands along the EFPC stream corridor. Thus, tributaries and diffuse sources (combined) accounted for 68% ± 10% (1SD) of flow at EFK5.0 in the dormant season and 59-62% ± 10% (1SD) of flow at EFK5.0 in the growing season (Table 1). Our snapshot estimates are in good agreement with recent data showing that 60% of annual baseflow hydrologic discharge at EFK5.0 was derived from tributaries and diffuse groundwater sources located throughout the watershed.[25] This simple hydrologic budget suggests that although the stream had smaller watershed contributions during August and October, tributaries and diffuse inputs contributed nearly 60% or more of stream water flow throughout the year.

Similar to stream water flow, average THg_d flux in April, August, and October at the Y12 boundary (EFK23.4; 12.7 ± 1.2 µg/s, 1SD) was typically smaller and less variable than downstream at EFK5.0 where THg_d flux ranged from 13.9 ± 1.8 µg/s (1SD) in April to an average of 18.8 ± 0.33 µg/s (1SD) in August and October (Table 1). Although tributary and diffuse sources (combined) contributed similar fractions of stream water flow during each of our seasonal sampling campaigns, the THg_d flux contributed by these sources varied substantially (Table 1). Maximum tributary contributions to THg_d flux during all seasons was minimal, on average representing only 1.1% ± 1.0% (1SD) of THg_d flux at EFK5.0. Some portion of this small maximum tributary THg_d flux is likely attributable to diffuse sources; however, because the maximum potential tributary THg_d flux is an order of magnitude smaller than estimated

diffuse fluxes and uncertainties (Table 1), tributary THg_d flux has no effect on the interpretation of diffuse fluxes. Calculated diffuse fluxes in April were also small, as well as relatively uncertain, representing only 6.3% ± 17.6% (1SD) of the THg_d flux at EFK5.0. In contrast, in August and October diffuse fluxes contributed substantially to THg_d loads at EFK5.0, accounting for 24% ± 16% (1SD) and 36% ± 15% (1SD) of THg_d fluxes at EFK5.0, respectively. This implies that high concentration diffuse sources of Hg can be an important *net* source of THg_d to the stream channel along the flow path of Lower EFPC. Diffuse sources of THg_d could be delivered to the stream via shallow, contaminated groundwater or alternatively, could be derived from the re-mobilization of legacy mercury associated with streambed sediment, as may be suggested by the very high THg_d concentrations of some hyporheic pore water samples (Table S2, Table S6). These results suggest that a greater complexity of Hg sources contribute to EFPC than previous findings of *Southworth et al*.[15, 16] that indicated present-day inorganic Hg inputs sustain waterborne Hg concentrations during baseflow. Moreover, whereas *net* fluxes reveal the balance of gains and losses of Hg along the flow path, such measurements cannot be used to assess whether turnover or exchange dynamics mask, in part, the magnitude of diffuse sources of THg_d along Lower EFPC.

THg_p fluxes at the Y12 boundary (EFK23.4; 39.3 ± 1.2 µg/s, 1SD) were also typically smaller and less variable than downstream at EFK5.0 where THg_p flux ranged from 52.7 ± 6.9 µg/s (1SD) in October, to 63.8 ± 8.3 µg/s (1SD) in April, and 111 ± 14.6 (1SD) µg/s in August (Table 1). Thus, approximately 25% ± 16% (1SD), 34% ± 16% (1SD), and 61% ± 14% (1SD) of the THg_p fluxes at EFK5.0 in October, April, and August, respectively, were derived from along the flow path, not including inputs from tributaries or the ORWTF (Table 1). Temporal differences in suspended sediment dynamics along EFPC may have been influenced by the timing of our longitudinal sampling in each season. In October, there was a longer period of baseflow conditions without event flow prior to sampling, whereas during August, sampling occurred immediately upon the return of baseflow subsequent to scouring high-flow conditions (Figure S1). *Southworth et al.*[15] suggested that biofilm accumulates suspended sediment from the water column along the flow path; thus, an increase in streambed biofilm may somewhat limit downstream transport of suspended sediment via physical retention, and therefore decrease the concentration of suspended THg_p along the flow path (e.g., suspended THg_p = 30.5 ng/L at EFK5.0 in October). In contrast, removal of biofilm by scouring high flow events may subsequently increase the amount of particulate-bound mercury that can be re-suspended along the flow path until the biofilm layer recovers (e.g., suspended THg_p = 114.8 ng/L at EFK5.0 in August).

Overall, our observations of hydrologic discharge in combination with mercury fluxes provide new insight into the sources of THg_d and THg_p being contributed to Lower EFPC, and the factors that control their variability. Our flux estimates suggest that diffuse legacy sources of Hg contamination (e.g., hyporheic discharge and riparian inputs) may contribute as much as a third of THg_d along the flow path of EFPC, depending on the season. In contrast, streambed dynamics (including biofilm) may significantly affect the transport and fate of the suspended

load along the flow path, as previously suggested.[15] Moreover, the magnitude of diffuse inputs of both THg_d and THg_p may be influenced by antecedent flow conditions. In the remainder of this paper, we utilize Hg isotope systematics to provide an independent assessment of the sources and processes influencing the transport, transformation, and fate of dissolved and particulate-bound Hg in the EFPC ecosystem.

3.3. Mercury Isotopic Composition in Stream Water

3.3.1. Suspended Particulate Hg Isotopic Composition. Suspended particulate-bound mercury (THg_p) δ^{202}Hg values ranged from -0.60‰ to 0.15‰ (±0.06‰, 2SD) and THg_p Δ^{199}Hg values ranged from -0.11‰ to 0.05‰ (±0.05‰, 2SD) (Table S4). Within Upper EFPC, THg_p was characterized by δ^{202}Hg and Δ^{199}Hg values (-0.42±0.09‰ δ^{202}Hg, 1SD, n=6; -0.01±0.02‰ Δ^{199}Hg, 1SD, n=6) that were similar to average commercial sources of liquid Hg^0 (-0.38±0.34‰ δ^{202}Hg, 1SD, n=13; near-zero Δ^{199}Hg), as summarized by *Sun et al.*[54] Downstream along the flow path, these THg_p Δ^{199}Hg and δ^{202}Hg values converged toward the isotopic composition of the < 125 µm fine-fraction of streambed sediment (δ^{202}Hg = 0.26‰ to -0.02‰; Δ^{199}Hg = -0.05‰ to -0.13‰)[34] (Figure 3). The convergence of suspended THg_p with the < 125 µm fine-fraction was consistent during all seasons, with the exception of the Δ^{199}Hg value associated with THg_p at EFK5.0 during April (Figure 3b). On average across multiple seasons we observed a 0.53‰ shift in δ^{202}Hg values and a -0.10‰ shift in Δ^{199}Hg values associated with suspended THg_p along the flow path of EFPC (Figure 3). Regression analysis combining isotopic data from both the < 2 mm and < 125 µm fractions [34] suggests that Δ^{199}Hg values associated with the streambed sediment also declined somewhat along the flow path ($p = 0.05$), whereas δ^{202}Hg values did not change significantly. The isotopic composition of streambed biofilm coatings was indistinguishable from the average isotopic composition of the suspended load at both upstream and downstream intensive sampling sites, similarly converging with the mercury isotopic composition of the streambed sediment (Figure 3, Table S5).

We cannot unequivocally identify the mechanisms responsible for the difference in Hg isotopic composition associated with the < 125 µm fine fraction of streambed sediment and the suspended THg_p from within Upper EFPC. It is possible that the isotopic composition of mercury released from Y12 has changed over time, as numerous remediation efforts have been made to decrease mercury exports from Y12.[14, 24, 49] However, historic source materials used within and discharged from Y12 were not available for isotopic analysis, and therefore we do not know whether remediation efforts altered the isotopic composition of Y12-derived mercury. If the isotopic composition of Y12-derived mercury has changed over time, then the Hg isotopic composition of the < 125 µm fine fraction of streambed sediment may simply result from the contribution of legacy sources to the streambed.

Mercury in the fine fraction of streambed sediment in Lower EFPC is thought to be derived predominantly from streambank erosion and, to a lesser extent, overland transport of floodplain soils.[15, 16, 49, 50] Moreover, a historic release deposit (HRD) layer has recently been observed in eroding streambanks within a limited number of highly localized reaches between

EFK22 and EFK18. This high concentration (~1,000 µg/g THg) layer of coal fines, fly ash, and Hg-rich precipitates was released from Y12 at the peak of industrial activities and deposited in floodplains of Lower EFPC.[50] Further research will be needed to quantify the Hg isotopic composition of streambank soil and the HRD to determine whether it differs from suspended THg_p in Upper EFPC, and if the isotopic composition of the < 125 µm fine fraction of streambed sediment could be derived from either of these legacy sources.

Alternatively, the isotopic composition of suspended THg_p in Upper EFPC may be a better approximation of the isotopic composition of mercury historically exported from Y12, as current elevated concentrations of mercury in stream water continue to be derived from metallic mercury historically lost to the local environment and oxidized mercury associated with neutralized nitric acid waste remaining within the Y12 storm drain network. The similarity in Hg isotopic composition of the suspended THg_p within Upper EFPC and commercial sources of liquid Hg^0 (see above) provides some support for this possibility. Moreover, *Donovan et al.*[34] showed that the δ^{202}Hg value of mercury in bulk (< 2 mm) sediment was negatively offset from the <125 µm fine fraction by up to -0.45‰, with bulk samples from EFK23 and EFK5 having the lowest δ^{202}Hg values (-0.23‰ and -0.28‰, respectively). It is possible that discrete coarse fractions, without the influence of finer fractions, may have a lower δ^{202}Hg value that approaches the composition of suspended particulates in Upper EFPC (-0.42±0.09‰ δ^{202}Hg, 1SD, n=6). This would suggest that coarser, less mobile size fractions more likely represent the signature of mercury historically released from Y12. In this case, the isotopic composition of mercury in the < 125 µm fine fraction of streambed sediment would need to be derived from processes that alter the isotopic composition of the historic source.

Donovan et al.[34] argued that in situ fractionation processes were unlikely to appreciably alter overall floodplain sediment Hg isotopic composition. However, it may be more plausible to significantly fractionate smaller pools of mercury associated with suspended THg_p, biofilm, and the < 125 µm fraction of streambed sediment. The < 125 µm fraction of streambed sediment likely constitutes < 10% of the larger inventory of mercury in bulk sediment in Lower EFPC (~ 172 kg to 289 kg in the < 1 mm to < 2 mm fraction, respectively), while the inventory of the < 125 µm fraction associated with the biofilm layer has been estimated to be even smaller (0.3 kg).[15, 16, 49] In comparison, the annual export of suspended THg_p from Y12 was ~3 kg during this study (coarsely estimated as 80% of annual total mercury fluxes across the Y12 boundary at EFK23.4). Using the Rayleigh equation and average fractionation factors for microbial reduction (α = 1.00163; Kritee et al. 2007) and photochemical reduction from thiol ligands (α = 1.00132),[55] we estimated that the -0.53‰ shift in δ^{202}Hg values between suspended THg_p and the <125 µm fraction of streambed sediment could result from mercury losses of ~28% via microbial reduction, and that losses of only ~10% would be required for photochemical reduction to impart the -0.10‰ shift in Δ^{199}Hg values associated with these relatively small inventories.

Overall, it is likely that some combination of these source-driven and process-driven mechanisms result in the consistent pattern of suspended THg_p isotopic convergence with the <

125 µm fine-fraction of streambed sediment along the flow path during all seasons. Given the growing understanding of the potential importance of streambank soils in replenishing streambed sediment in EFPC,[15, 16, 49, 50] it is possible that streambank soils contribute mercury with an isotopic composition having intermediate δ^{202}Hg values between that of suspended THg_p from Upper EFPC and the < 125 µm fraction of streambed sediment from Lower EFPC. It is also possible that Y12-derived inputs from THg_p in Upper EFPC and streambank soils are further processed within the streambed sediment (and biofilm), progressively imparting them with small negative Δ^{199}Hg values along the flow path. Thus the isotopic composition of the THg_p converges with the < 125 µm fine fraction of streambed sediment as suspended particulates spiral downstream[56], being repeatedly deposited to, processed within, and re-suspended from the biofilm layer, and mix with progressively more altered fine sediment along the flow path. The suspended particulates likely integrate isotopic signals over longer reaches than does the streambed sediment, and the biofilm further temporally integrates the suspended particulate signal leading to its extraordinarily consistent isotopic composition at each intensive site along the flow path. A more detailed study of Hg isotopes in streambed sediment size fractions, the streambank soil, and the HRD layer along the flow path of EFPC will be required to further assess this conceptual model.

3.3.2. Dissolved Hg Isotopic Composition. Stream water total dissolved mercury (THg_d) had δ^{202}Hg values ranging from -0.44‰ to 0.18‰ (±0.06‰, 2SD) and THg_d Δ^{199}Hg values ranging from -0.02‰ to 0.24‰ (±0.05‰, 2SD) (Table S1). Based on predominantly near-zero Δ^{200}Hg and Δ^{204}Hg values of THg_d and THg_p, even-mass-MIF in stream water was negligible. The Δ^{199}Hg and δ^{202}Hg values associated with THg_d underwent less consistent shifts along the flow path than those associated with particulates in both Upper and Lower EFPC (Figure 4). Although the initial THg_d δ^{202}Hg values in Upper EFPC varied from -0.44‰ to 0.18‰, they converged to an average value of -0.01‰ (± 0.10‰, 1SD) during all seasonal sampling periods (Figure 4a). In contrast, initial THg_d Δ^{199}Hg values were narrowly clustered, displaying near-zero Δ^{199}Hg values consistent with commercial sources of metallic mercury, similar to THg_p (Figure 4). Unlike in the particulate phase, these dissolved phase Δ^{199}Hg values underwent small and directionally variable changes along the flow path, although dynamics were strikingly consistent within most individual reaches of EFPC. While this pattern is notable for its consistency across seasons, and may reflect some consistency in biogeochemical processes (e.g., photochemical reduction), environmental data was not available at high enough temporal and spatial resolution to evaluate correlations between observed MIF and potential drivers (e.g., canopy shading, cloud cover). Nevertheless, the δ^{202}Hg and Δ^{199}Hg values of THg_d suggest differences in the processes impacting MDF and MIF. Historic and ongoing activities within Y12 appear to result in variable MDF prior to release into EFPC, possibly due to variations in the isotopic composition of various mercury sources within Y12, whereas processes affecting Δ^{199}Hg values only occur subsequent to discharge into EFPC. The observation that widely varying starting THg_d δ^{202}Hg values converged to a relatively narrow range of values along the flow

path, increasing in October and August and decreasing in April, suggests that additional source input(s) may have a predominant influence on THg_d $\delta^{202}Hg$ values downstream of Y12, whereas, THg_d $\Delta^{199}Hg$ values appear to be predominantly influenced by a similar set of biogeochemical transformations across all seasons.

Overall, the observation that mercury isotopic composition associated with suspended solids and in the dissolved phase changed along the flow path of EFPC and among seasonal sampling periods broadly demonstrates that decreases in mercury concentrations along the flow path could not have resulted exclusively from the physical processes of dilution and sedimentation. That is, in order to shift the isotopic composition of waterborne mercury, mercury must be either lost or gained from a given fraction. Moreover, changes in the isotopic composition of THg_d and THg_p were not expressed as monotonic systematic shifts along the flow path based on dual isotope plots of $\Delta^{199}Hg$ and $\delta^{202}Hg$ values (Figure S3). Whereas the dual isotope plot of THg_p $\Delta^{199}Hg$ and $\delta^{202}Hg$ values did generally decrease in $\Delta^{199}Hg$ values and increase in $\delta^{202}Hg$ values over the ~ 20 km flow path, the plot of THg_d $\Delta^{199}Hg$ and $\delta^{202}Hg$ values along the flow path was seemingly erratic within and among the seasonal sampling periods (Figure S3). This decoupling of $\Delta^{199}Hg$ and $\delta^{202}Hg$ values suggests that no single biogeochemical process or additional source input alone results in the observed THg_d and THg_p concentrations and shifts in isotopic composition along the flow path, but rather, a complex suite of biogeochemical transformations and/or source input(s) likely influence stream water mercury concentrations and isotopic composition in Lower EFPC.

3.4. In-Stream Processes and Additional Source Inputs.

Mercury isotopes fractionate in the natural environment through photochemical, biotic, and dark abiotic pathways.[13] Overall, Hg isotope fractionation can impart distinct isotopic signatures within various environmental pools that serve as both a record of biogeochemical cycling, and as a tracer of subsequent mobilization and transport. Here we use observed changes in $\Delta^{199}Hg$ and $\delta^{202}Hg$ values associated with suspended solids (THg_p) and the aqueous dissolved phase (THg_d) along the flow path of EFPC to further constrain the relative importance of various in-stream processes (e.g., mercury reduction, microbial methylation and demethylation, and partitioning among dissolved and particulate phases) and additional source(s) of mercury (e.g., non-Y12-impacted tributaries, the hyporheic zone, and riparian wetlands) in Lower EFPC.

Our approach is first to assess whether in-stream processes can plausibly account for observed shifts in THg_d and THg_p isotope composition along the flow path, and second to consider the potential influence of additional source(s), as suggested by our assessment of hydrologic mercury fluxes (see section 3.2). We acknowledge that additional source inputs along the flow path could somewhat confound our attempt to assess process-level influences on waterborne THg_d and THg_p isotope composition; however, because $\delta^{202}Hg$ and $\Delta^{199}Hg$ along the flow path are decoupled, our observations cannot be explained through mixing alone, and thus in-stream biogeochemical processing must also be considered. Although this approach may not allow the unequivocal identification of the mechanism(s) responsible for observed shifts in Hg

isotopic composition, it allows us to better constrain the possibilities and thus should lead to an improved understanding of Hg biogeochemical cycling in EFPC and other lotic ecosystems.

3.4.1. Mercury Reduction Processes. Recent experiments investigating photochemical and dark abiotic and biotic oxidation and reduction pathways with natural waters and substrates have demonstrated that various redox processes could influence Hg cycling in EFPC[44, 57-61] However, the relative rates of these processes are dependent upon environmental conditions and thus, it is challenging to predict which processes most influence the biogeochemical cycling of mercury *in situ*. Using mercury isotopes, we can assess if any previously characterized redox pathways are influential *in situ* in EFPC.

The Δ^{199}Hg values associated with both the dissolved and particulate fractions display only subtle changes downstream of Y12 (see section 3.3) (Figure 3, Figure 4). Such small changes in Δ^{199}Hg values suggest that photochemical transformations are of only minor significance within Lower EFPC.

Photochemical reduction of mercury in natural waters of EFPC could occur within the aqueous phase or on surfaces of the suspended fraction. Mercury is primarily bound to reduced sulfur ligands within EFPC,[22, 23, 57, 61, 62] and so we focus our discussion on the isotopic effects of photochemical reduction of mercury primarily bound to sulfur ligands. Photochemical reduction of mercury from sulfur bearing ligands in the aqueous phase, with subsequent evasion from the water column, would decrease the Δ^{199}Hg value of the remaining aqueous oxidized pool.[55] Thus, photochemical reduction from the dissolved phase is not consistent with shifts in Δ^{199}Hg values of THg_d observed in Lower EFPC (Figure 4b).

Photochemical reduction of mercury from sulfur bearing ligands in the suspended phase would decrease the Δ^{199}Hg values of the remaining suspended phase, which is consistent with observed trends along the flow path (Figure 3b). Simultaneously, reduced mercury released to the water column would increase the Δ^{199}Hg value of the dissolved phase temporarily until the released DGM was either volatilized or re-oxidized and re-adsorbed (Figure 4b). If DGM released from the suspended phase was quantitatively volatilized from the water column, the dissolved phase would exhibit a transient increase in Δ^{199}Hg values that subsequently return to the initial near-zero Δ^{199}Hg values of Upper EFPC. On the other hand, if a fraction of this released DGM was photochemically re-oxidized and re-adsorbed, the *net* overall effect would still be a decrease in Δ^{199}Hg values associated with the suspended phase, and only a transient shift would be observed in the aqueous phase. Photochemical reduction of mercury from sulfur-bearing ligands would also increase δ^{202}Hg values of the residual suspended phase, and this is directionally consistent with the isotopic composition of the suspended load along the flow path (Figure 3a). Photochemical reduction from sulfur bearing ligands within the streambed biofilm coatings would result in similar effects. However, photochemical reduction of mercury from sulfur bearing ligands has a characteristic Δ^{199}Hg:δ^{202}Hg ratio of about -0.8[55]. Thus, given the observed small decrease in Δ^{199}Hg of the suspended phase (~ -0.10‰), we would expect to see only a small concomitant increase in the δ^{202}Hg value of the suspended phase (~0.13‰). In

contrast, we observed a 0.53‰ increase in δ^{202}Hg values associated with the suspended phase, and thus photochemical reduction could only account for ~20% of MDF recorded in THg_p. Therefore, additional processes are required to account for the observed increases in δ^{202}Hg values associated with the suspended phase, that could occur in part within the streambed biofilm as the suspended load spirals downstream,[56] being repeatedly deposited, re-suspended, and further processed along the flow path (Figure 3).

There are several non-photochemical (i.e., dark) biotic and abiotic mechanisms that could additionally increase the δ^{202}Hg values of residual Hg(II) of the suspended phase and streambed biofilm, including microbial methylation,[63] dark abiotic reduction,[64] and microbial reduction.[65, 66] The concentrations of MeHg in surface waters of the EFPC ecosystem are low, especially relative to total mercury concentrations (i.e., %MeHg, Table S3). Thus, it seems unlikely that contributions of MeHg could significantly shift the isotopic composition of the large residual inorganic mercury pool. Moreover, the small Δ^{199}Hg values associated with waterborne THg_d and THg_p, and sediment, suggest that photochemical demethylation is not a driving process within EFPC. Thus, dark abiotic reduction and/or microbial reduction may be more likely responsible for the additional MDF observed in the suspended phase along the flow path.

Dark abiotic reduction and volatilization from the stream water dissolved fraction would increase δ^{202}Hg and decrease Δ^{199}Hg values of the residual aqueous phase.[64] Although we observed increases in δ^{202}Hg values of the dissolved fraction along the flow path in August and October, these shifts did not occur consistently across all seasonal sampling periods (Figure 4a). Moreover, we observed transient increases in Δ^{199}Hg values, opposite of what would be expected if dark abiotic reduction from the dissolved fraction was a dominant process (Figure 4b). Thus dark abiotic reduction of mercury from the dissolved phase does not likely drive observed shifts in mercury isotopic composition of stream water along the flow path.

Dark abiotic reduction of mercury from the suspended phase would increase δ^{202}Hg values of the residual suspended phase, which is consistent with observed increases in δ^{202}Hg values associated with the particulate fraction along the flow path during all seasonal sampling periods (Figure 3a).[64] This process would also result in small decreases in the Δ^{199}Hg values of the suspended load, and released Hg(0) would transiently increase Δ^{199}Hg values of the dissolved fraction, both of which are consistent with our observations (Figure 3b, Figure 4b).[64] Dark abiotic reduction has a characteristic Δ^{199}Hg: δ^{202}Hg ratio of about -0.12.[64] Thus, even the subtle decrease in Δ^{199}Hg observed within the suspended phase (~0.10‰) would be associated with a large shift in δ^{202}Hg values of ~0.82‰, which would more than account for the ~0.53‰ increase in δ^{202}Hg values of THg_p. Thus, dark abiotic reduction alone could account for the observed MDF within the particulate phase, but would be constrained to account for no more than ~60% of the odd-mass-number MIF (i.e., Δ^{199}Hg) recorded in THg_p.

Based on observed MDF and MIF along the flow path and experimentally derived Δ^{199}Hg: δ^{202}Hg ratios, a combination of photochemical reduction and dark abiotic reduction could account for observed isotopic shifts along the flow path, with dark abiotic reduction accounting for ~60% of the shift in Δ^{199}Hg values and ~90% of the shift in δ^{202}Hg values within

the suspended particulate fraction. However, mechanisms that induce MIF can also be differentiated by the $\Delta^{199}Hg$:$\Delta^{201}Hg$ ratio. Although this assessment is difficult for delta values < ± 0.3‰,[13] the odd-mass-number MIF observed in the suspended particulate fraction of EFPC stream water had a $\Delta^{199}Hg$:$\Delta^{201}Hg$ slope of 0.98 (± 0.18, 1SE; n = 24; $p<0.0001$; $r^2=0.59$) that appeared to be more influenced by photochemical reduction ($\Delta^{199}Hg$:$\Delta^{201}Hg$ ratio of ~ 1.0) than by dark abiotic reduction ($\Delta^{199}Hg$:$\Delta^{201}Hg$ ratio of ~ 1.6) (Figure S4).[64, 67, 68] Thus, the predominant role of dark abiotic reduction required for these two processes to account for observed shifts in $\Delta^{199}Hg$ and $\delta^{202}Hg$ values is not consistent with characteristic ratios of odd-mass-number MIF. Although dark abiotic reduction may play a role in the biogeochemical cycling of Hg in EFPC, it does not appear to explain observed mercury isotope dynamics along the flow path.

Microbial reduction releases Hg(0) with lower $\delta^{202}Hg$ values than the residual substrate, without affecting MIF.[65, 69] Whether this process occurs within the suspended phase, or *in situ* within streambed biofilm and subsequently Hg is re-mobilized to the water column, the effect would be increasing $\delta^{202}Hg$ values associated with the suspended phase and/or biofilm along the flow path of EFPC, without any additional influence on $\Delta^{199}Hg$ values. Thus, while the observed shift in THg_p $\Delta^{199}Hg$ values constrains photochemical reduction to account for only ~20% of the shift in THg_p $\delta^{202}Hg$ values, microbial reduction could account for the remaining ~80% of the observed 0.53‰ shift in THg_p $\delta^{202}Hg$ values. Given the low concentration of DGM in the water column of Lower EFPC, reduced mercury contributed to the aqueous phase is likely volatilized from the stream or is rapidly re-oxidized and re-adsorbed to the suspended phase or streambed biofilm. Thus, microbial reduction processes could conceivably influence the isotopic composition of the suspended phase and biofilm without influencing the isotopic composition of the dissolved phase. Microbial reduction of mercury from the suspended phase and/or streambed biofilm is consistent with our observations of isotopic composition (Figure 3a) and decreases in mercury concentration of the suspended phase along the flow path of EFPC (Table S3, Figure 3c), despite that recent laboratory studies suggest that binding of Hg(II) with thiols and sulfides inhibits microbial reduction.[70] Nonetheless, highly contaminated substrates, as are found within EFPC, are likely sites for microbial reduction[71, 72] and microbial dynamics may be less seasonally impacted than photochemical mechanisms that may be limited by tree canopy shading.

In summary, various pathways of mercury reduction provide mechanisms that could reasonably result in the observed $\Delta^{199}Hg$ values of the dissolved phase, and both $\Delta^{199}Hg$ and $\delta^{202}Hg$ values of the suspended phase. Photochemical reduction of sulfur-bound mercury from the suspended fraction, coupled with subsequent volatilization and/or re-oxidation and re-adsorption appears to be consistent with observed variation in the $\Delta^{199}Hg$ values in both the dissolved and suspended phases along the flow path. However, this photochemical process cannot alone explain the magnitude of $\delta^{202}Hg$ shifts along the flow path of EFPC. Photochemical reduction in combination with dark abiotic reduction could account for the observed shifts in both $\Delta^{199}Hg$ and $\delta^{202}Hg$ values within the particulate fraction. However, this

requires that the observed MIF is predominantly driven by dark abiotic reduction (~60%), and this is not consistent with the observed $\Delta^{199}Hg$:$\Delta^{201}Hg$ ratio within the particulate fraction. Thus, alternatively, microbial reduction of mercury within the suspended phase and streambed biofilm, followed by volatilization and/or re-oxidation of released DGM, may more likely be the predominant mechanism leading to increasing $\delta^{202}Hg$ values in the suspended phase.

Thus, reduction processes are able to account for observed mercury isotope variations associated with $\Delta^{199}Hg$ values of the dissolved phase and both $\Delta^{199}Hg$ and $\delta^{202}Hg$ values of the suspended phase. Similarly, *Foucher et al.*[73] suggested that non-photochemical reduction was a dominant mechanism of Hg removal from a gold mining impacted stream in Canada, subsequent to degradation of unstable Hg-cyanide complexes. However, our assessment of isotopic fractionation during redox reactions does not suggest a mechanism for the lack of consistency of dissolved phase $\delta^{202}Hg$ values along the flow path among different seasons, and we therefore suggest that there must be an additional mechanism(s) that influence mercury dynamics within the EFPC stream ecosystem.

3.4.2. Partitioning Dynamics. Mercury partitioning between dissolved and particulate phases may be influenced by both kinetic and equilibrium processes. During kinetically controlled mass dependent fractionation of Hg isotopes, lighter isotopes would be expected to preferentially enrich the particulate phase. For example, precipitation of montroydite (HgO) was shown to be under kinetic control and displayed a $\varepsilon^{202}Hg_{(precipitate\text{-}supernatant)}$ enrichment factor of -0.32‰.[74] Equilibrium Hg isotope fractionation during adsorption, complexation, and precipitation processes also has been shown to enrich the residual dissolved phase in heavier isotopes (increasing $\delta^{202}Hg$ values), relative to the adsorbed, complexed, or precipitated phase that becomes enriched in lighter isotopes.[73-76] Equilibrium experiments for Hg(II)-sorption to goethite,[76] Hg(II)-thiol complexation,[75] and metacinnabar (β-HgS) precipitation[74] were characterized by enrichment factors ($\varepsilon^{202}Hg_{(particulate\text{-}dissolved)}$) ranging from -0.53 ± 0.15‰ (2SD) to -0.67‰ ± 0.08 (2SD). Although these studies suggest that dissolved Hg speciation and aqueous ligand exchange are important controls on equilibrium Hg isotope fractionation, the ultimate effect of Hg(II) partitioning to particulate phases appears to be similar across a range of environmentally relevant processes.[74]

In our field-based study, $\delta^{202}Hg$ values associated with THg_d increased along the flow path of EFPC during October and August (Figure 4a), consistent with fractionation processes during partitioning between dissolved and particulate phases. If kinetic and/or equilibrium fractionation during partitioning of Hg was controlling the increase in THg_d $\delta^{202}Hg$ values along the flow path of EFPC, particulate phase $\delta^{202}Hg$ values would also be expected to increase, but with a negative $\delta^{202}Hg_{(p\text{-}d)}$ offset relative to the dissolved phase. Although THg_p $\delta^{202}Hg$ values did increase along the flow path of EFPC (Figure 3a), we did not observe a consistent negative $\delta^{202}Hg_{(p\text{-}d)}$ offset between the dissolved and particulate phases (Figure 5). In April, THg_d behaved differently than in August and October, displaying an overall decrease in $\delta^{202}Hg$ values along the flow path while THg_p $\delta^{202}Hg$ values increased similarly during all three sampling periods. On

one hand, these observations could be interpreted to mean that adsorption dynamics are not a dominant control over isotopic effects in EFPC. On the other hand, it is possible that other factors such as co-occurring reactions or the mass balance between the dissolved and suspended phases are simply obscuring the expected isotopic effects of partitioning processes.

In-field observations may be complicated by co-occurring interactions among dissolved inorganic Hg species, dissolved Hg-NOM complexes, and particulate-bound Hg phases. *Miller et al.*[23] scrutinized the complexation of mercury with dissolved NOM in Upper EFPC (EFK26.0 to EFK23.4). Their experiments suggested an initial rapid interaction of a portion of dissolved inorganic Hg with dissolved NOM in Upper EFPC, followed by slower kinetically controlled Hg-NOM reactions. *Miller et al.*[23] suggested that during the slower kinetically controlled phase of this Hg-NOM interaction, Hg was being transferred from inorganic complexes or weak Hg-NOM complexes (e.g., carboxyl and amine functional groups) to stronger Hg-NOM complexes (e.g., hydrophobic moieties with mono- or bi-dentate binding with thiol functional groups) within the macromolecular structure of dissolved NOM. Complexation experiments done with both Hg-spiked and non-spiked natural stream water from EFPC did not achieve equilibrium within 24 hours.[23] This is similar to the long equilibration times (1 to > 30 days) observed by *Jiskra et al.*[77] for the interaction of various dissolved aqueous Hg species with carboxyl- and thiol-resins. For comparison, the time required for stream water to travel from the Y12 boundary (EFK23.4) to our furthest downstream sampling site (EFK5.0) at base flow is ~48 hours.

Based on a mass balance of reducible and non-reducible fractions, *Miller et al.*[23] also suggested that Hg that did not initially form strong Hg-NOM complexes was more likely to be particle reactive. Using X-ray fluorescence (XRF) mapping, *Gu et al.*[22] showed that particulates in Upper EFPC were a mixture of diatoms and mineral particles, with Hg being most associated with sulfhydryl groups on NOM-coated iron-oxyhydroxide mineral particulates.

Thus, in both the dissolved and suspended particulate phases in EFPC, reduced sulfur in natural organic matter likely plays a key role in Hg complexation. Taken together, the complexity of co-occurring interactions among dissolved inorganic Hg species, dissolved Hg-NOM complexes, and particulate-bound Hg phases; slow equilibration processes; and evidence of additional THg_d inputs from diffuse legacy sources (see section 3.2), and inorganic Hg inputs due to mercury reduction from substrates along the flow path (see section 3.4.1), likely obscure our ability to observe expected isotopic effects derived from controlled adsorption, complexation, and precipitation experiments.

Washburn et al.[78] observed a positive $\delta^{202}Hg_{p\text{-}d}$ offset between dissolved and suspended phases in point-source Hg-contaminated stream water from the South River in Virginia, USA (mean = 0.29 ± 0.16‰ (1SD); min = 0.09‰; max = 0.58‰; as calculated from data tables). Note that we have reversed the sign convention reported in *Washburn et al.*[78] to follow *Jiskra et al.*[76] and *Smith et al.*[74] This $\delta^{202}Hg_{p\text{-}d}$ offset was opposite in sign to that expected based on adsorption, complexation, and precipitation experiments.[73-76] The authors suggested that there was an initial rapid reaction between released Hg and a limited quantity of reduced sulfur moieties associated with filter-passing colloidal organic matter that imparted relatively negative $\delta^{202}Hg$ values to the

colloidal phase, and that the residual dissolved Hg with relatively more positive $\delta^{202}Hg$ values subsequently partitioned to the suspended phase.[78] This proposed mechanism is consistent with the complexation dynamics demonstrated by *Miller et al.*[23] with reducible and non-reducible Hg fractions in Upper EFPC, except that *Miller et al.*[23] suggested that the initial rapid complexation occurred between released inorganic Hg complexes and dissolved NOM.

In our study, across all seasons, we did not observe a consistent negative $\delta^{202}Hg_{p\text{-}d}$ offset representative of kinetic and/or equilibrium fractionation experiments, nor did we see a consistent positive $\delta^{202}Hg_{p\text{-}d}$ offset representative of the dissolved phase Hg-DOM complexation mechanism suggested by *Washburn et al.*[78] Instead, the direction and magnitude of the $\delta^{202}Hg_{p\text{-}d}$ offset varied among seasonal sampling periods and along the flow path of EFPC (Figure 5). In October, when hydrologic flows were the lowest, we observed positive $\delta^{202}Hg_{p\text{-}d}$ offsets that increased from 0.01 to 0.33‰ along the flow path from Upper EFPC downstream to EFK5.0, at which point the $\delta^{202}Hg_{p\text{-}d}$ offset dropped suddenly to -0.06‰. In April, when hydrologic flows were highest, we observed the most negative $\delta^{202}Hg_{p\text{-}d}$ offsets in Upper EFPC that then gradually increased to positive values along the flow path of Lower EFPC (Figure 5). Altogether, $\delta^{202}Hg_{p\text{-}d}$ offsets ranged from negative to near-zero values along Upper EFPC, and increased to positive values downstream along Lower EFPC ($p < 0.01$, $r^2 = 0.44$, $n = 23$, excluding one outlier at EFK5.0 in October). This may suggest that mechanisms reflective of kinetic and/or equilibrium Hg fractionation experiments are more dominant in the upper reaches of EFPC, but that the dissolved phase Hg-DOM complexation mechanism proposed by *Washburn et al.*,[78] is more dominant in the lower reaches of EFPC. Validating the mechanism responsible for observed positive $\delta^{202}Hg_{p\text{-}d}$ offsets will require additional targeted, controlled experiments. Nonetheless, the shifting magnitude and sign of the $\delta^{202}Hg_{p\text{-}d}$ offset may suggest additional inputs of dissolved Hg along the flow path, as additional sources of mercury contributed to the water column may be more reactive. Mercury reduction pathways that potentially drive observed $\Delta^{199}Hg$ and $\delta^{202}Hg$ values of the suspended THg_p (see section 3.4.1) would provide an ongoing source of dissolved gaseous mercury to the water column as the suspended load spirals downstream, being repeatedly deposited, re-suspended, and progressively processed along the flow path. Moreover, the addition of dissolved Hg into the stream channel is consistent with our hydrologic and Hg flux estimates that indicate non-Y12-impacted tributaries and diffuse legacy sources (e.g., hyporheic discharge and riparian wetland inputs) contribute as much as a third of the THg_d along the flow path of EFPC (see section 3.2).

Despite trends in $\delta^{202}Hg_{p\text{-}d}$ offsets, the mass balance of mercury between dissolved and suspended phases along the flow path makes it unlikely that partitioning processes are a dominant control on mercury isotope dynamics in EFPC. If adsorption of Hg from the dissolved to the particulate phase was a dominant process controlling concentrations of mercury in the water column, we would have expected that as THg_d concentrations decreased along the flow path, THg_p concentrations would have increased. On a mass-volume basis, THg_d concentrations decreased by 38 ng/L (± 5 ng/L, 1SD), which is significant relative to the 66 ng/L (± 44 ng/L, 1SD) THg_p concentrations at EFK5.0, and therefore a transfer of this amount of Hg from the

dissolved to particulate fraction would likely be measurable. However, THg_p concentrations simultaneously decreased by 94 ng/L (± 55 ng/L, 1SD) on a mass-volume basis and by 33 µg/g (± 9 µg/g, 1SD) on a mass-mass basis. Thus, regardless of the effect of diluting waters, THg_p concentrations decrease, not increase, along the flow path. Although this assessment may be somewhat confounded by the incorporation of sediment with lower Hg concentrations along Lower EFPC, adsorption dynamics do not appear to be the primary driver of waterborne Hg concentrations or isotopic composition along the flow path of EFPC.

3.4.3. Tributary, Hyporheic, and Riparian Inputs. In-stream biogeochemical transformations cannot account for the seasonally variable shifts in mass-dependent mercury isotope values associated with the dissolved phase along the flow path of EFPC (Figure 4a). Therefore, it is likely that additional source inputs from the watershed downstream of Y12 also influence mercury dynamics within the Lower EFPC ecosystem. Additional sources of dissolved mercury to EFPC could include stream water contributions from non-Y12-impacted tributaries, or diffuse inputs of pore water and shallow groundwater from the hyporheic zone and adjacent riparian floodplains.

Tributary and reference site THg_d concentrations were typically < 1.0 ng/L, which was insufficient for mercury isotope analysis. However, the isotopic composition of tributary sediment (δ^{202}Hg = -0.84 to -3.22‰),[34] reference site streambed sediment (δ^{202}Hg = -1.42‰),[34] and reference site streambed sediment associated with hyporheic pore water samples (δ^{202}Hg = -1.26 to -1.38‰), all consistently displayed much lower δ^{202}Hg values than observed for sediment in EFPC. Evidence from non-point-source impacted lakes, streams, and forest runoff suggest that THg_d in these tributaries should have similar or lower δ^{202}Hg values than associated sediment and soils.[79, 80] *Jiskra et al.*[80] showed that the isotopic composition of THg_d in boreal forest runoff was similar to the organic soils from which it originated, with THg_d δ^{202}Hg values ranging from -2.29 to -1.76‰. *Chen et al.*[79] directly compared the isotopic composition of sediment and filtered surface water of non-point-source impacted lakes in Ontario, Canada. In their study, lake sediment δ^{202}Hg values ranged from -1.24 to -0.68‰, while filtered surface water THg_d δ^{202}Hg values were even lower, ranging from -1.96 to -1.27‰; one filtered stream water sample had a THg_d δ^{202}Hg value of -2.22‰ ± 0.15‰ (2SD).[79] Thus, given these soil-runoff and sediment-surface water comparisons, and the very low δ^{202}Hg values of tributary and reference site sediment in our study, it is unlikely that tributaries could have THg_d δ^{202}Hg values high enough to drive EFPC THg_d toward the near-zero δ^{202}Hg values observed at our furthest downstream site (EFK5.0, mean THg_d δ^{202}Hg = -0.01‰ ± 0.10‰, 1SD).

Whereas *Jiskra et al.*[80] suggested that forest soil runoff originated from Hg associated with litter inputs to the forest soils, *Chen et al.*[79] suggested lake surface water isotopic composition was also influenced by precipitation. North American measurements of precipitation from relatively nonlocally-impacted sites have δ^{202}Hg values ranging from -1.59 to 0.21‰.[45, 81-84] Moreover, tributaries contributed only 0.6 to 1.7% of the THg_d flux at EFK5.0 (Table 1, Figure 2), so even if we assumed that all tributary THg_d in the region was derived

directly from the most positive δ^{202}Hg values for precipitation, which is highly unlikely given the proximity of coal fired utility boilers,[34, 82] non-Y12-impacted tributaries could not have an observable effect on the THg_d isotopic composition in EFPC.

Flux calculations suggest that diffuse sources such as inputs from the hyporheic zone and riparian floodplains contributed up to 36% ± 15% (1SD) of THg_d to EFPC (Table 1, Figure 2) (see section 3.2). Diffuse hyporheic and riparian sources could include discharges of Hg-contaminated shallow groundwater or re-mobilization of legacy mercury from contaminated streambed sediment or floodplain soils. Recent inventories and sequential extractions of Hg in streambed sediment in EFPC suggest that re-mobilization of legacy sources could significantly contribute to stream water THg_d loads. The current inventory of Hg in EFPC streambed sediment was estimated to be 334 kg.[49] Although most Hg in streambed sediment is strongly bound, 0.18 – 0.30% (interquartile range) was extractable by de-ionized water (calculated with data from *Brooks et al.*[49]). Combining inventory and extraction data, we calculated that 0.6 -1.0 kg of legacy mercury in streambed sediment was weakly bound and could be potentially re-mobilized to the aqueous phase. In comparison, the THg_d flux at EFK5.0 during water year 2013 was 0.368 kg/yr at baseflow, and 1.003 kg/yr during baseflow and stormflow combined.[25] Importantly, recent estimates suggest that streambank soils annually contribute ~53 kg of THg to streambed sediment,[15] and thus water-soluble sources of legacy Hg may be replenished frequently. Altogether, this indicates that re-mobilization of legacy Hg from streambed sediment could be a sustainable source of Hg to stream water.

Hyporheic pore water at our upstream and downstream intensive sampling sites within EFPC (i.e., EFK22.3, and EFK5.0, respectively) was characterized by δ^{202}Hg values that were typically similar to or higher than δ^{202}Hg values of overlying stream water (Table S5; Figure 6, Figure S5). Hyporheic pore water THg_d concentrations ranged from being lower than to greatly exceeding overlying stream water, ranging from 6.6 ng/L to 5,000 ng/L at EFK22.3, and from 2.3 ng/L to 60.5 ng/L at EFK5.0 (Table S2, Table S6). In contrast, surface water and pore water emanating from a Y12-impacted riparian wetland at EFK22.3 had δ^{202}Hg values that were typically similar to or lower than δ^{202}Hg values of adjacent stream water (Table S5; Figure 6; Figure S5). Riparian pore water THg_d concentrations did not typically exceed adjacent surface water THg_d concentrations, ranging from 5.4 ng/L to 53.7 ng/L at EFK22.3 (Table S2, Table S6). Altogether, this suggests that mixing or exchange of stream water with hyporheic pore water is a possible explanation for increasing δ^{202}Hg values downstream along EFPC during October and August when EFPC is less hydrologically connected with the watershed.

During April, shifts in mercury isotope values along the flow path of EFPC were different than in August and October. During the April sampling period, the farthest upstream δ^{202}Hg value of THg_d in stream water was significantly higher than during August and October, rapidly declining to a near-zero δ^{202}Hg value while still within the channelized Upper EFPC (Figure 4a). Downstream of the Y12 boundary at EFK23.4, δ^{202}Hg values of the dissolved phase did not markedly change along the flow path of Lower EFPC. This likely reflects minimal diffuse THg_d inputs to EFPC in April, despite the observation that discharge from tributaries and

diffuse sources (combined) was 45% ± 3% (1SD) greater than in August and October (Table 1). Diffuse THg_d inputs to EFPC may have been minimal in April due to high antecedent flow conditions (20.5 m^3/s peak stormflow discharge, relative to 1.22 m^3/s baseflow discharge) two weeks prior to sampling that may have had a flushing effect on the hyporheic zone. This was a significant but not atypical high flow event, having a return interval of 1.05 – 1.25 years, with only three to four events per year, on average, having flows as high or higher. Moreover, any small THg_d flux with higher $\delta^{202}Hg$ values contributed from the hyporheic zone may have been offset by contributions with lower $\delta^{202}Hg$ values from riparian wetlands during this period when EFPC was more hydrologically connected to the watershed.

Ancillary stream water chemistry along the flow path in conjunction with ancillary pore water chemistry from the hyporheic zone and riparian wetlands is consistent with our hypothesis that diffuse hydrologic inputs influence stream water composition along the flow path of EFPC. Although variable, DOC concentrations and $SUVA_{254}$ values in upstream and downstream hyporheic zones and riparian wetlands were typically similar to or greater than values in adjacent surface waters in the upper and lower reaches of EFPC (Table S3, Table S6), making it plausible that hydrologic contributions from these reservoirs could increase DOC concentrations and $SUVA_{254}$ values along the flow path. Dissolved organic carbon (DOC) increased with distance downstream during August ($p < 0.01$, $r^2 = 0.79$, $n = 8$) and October ($p = 0.02$, $r^2 = 0.62$, $n = 8$), but not in April ($p = 0.14$, $n = 8$). Similarly, $SUVA_{254}$ also increased along the flow path in August ($p < 0.01$, $r^2 = 0.85$, $n = 8$) and October ($p < 0.01$, $r^2 = 0.91$, $n = 8$), but not during April ($p = 0.62$, $n = 8$) when $SUVA_{254}$ values were more variable but remained relatively high throughout EFPC (Figure 7, Table S3). Thus, it is not surprising that DOC and $SUVA_{254}$ were strongly correlated in August and October ($p < 0.01$, $r^2 = 0.79$, $n = 16$), but not in April ($p = 0.173$, $n = 8$) (Figure 7). Altogether, this suggests that in August and October, the DOC that is contributed to the water column along the flow path is increasingly more aromatic, reflective of greater terrestrially derived sources from the watershed.[8, 11, 25, 85] In April, it appears that stream water became more influenced by terrestrially derived carbon within Upper EFPC, perhaps from flow management waters imported from the Clinch River, and $SUVA_{254}$ values remained high along the flow path of Lower EFPC, likely due to the continued addition of watershed-derived sources of DOC. In August and October, $SUVA_{254}$ values explained 81% and 69% of the variability in THg_d $\delta^{202}Hg$ values in stream water along the flow path ($p < 0.01$, $n = 8$ for August; $p = 0.01$, $n = 8$ for October). Overall, seasonal differences in hydrologic inputs and $SUVA_{254}$ were the only identified parameters that demonstrated seasonally distinct patterns along the flow path that were similar to the seasonally distinct patterns observed for THg_d $\delta^{202}Hg$ values. These results suggest that a significant amount of the variability in $\delta^{202}Hg$ values was controlled by hydrological processes that delivered terrestrially derived, more aromatic DOC to the stream channel from watershed sources, whereas much of the modification to odd-mass-MIF occurred within the stream channel (see section 3.4.1). Overall, our Hg isotope results are consistent with the generally accepted conceptualization that mercury mobilization and transport are intrinsically

linked to organic matter and hydrological dynamics, even within this point-source Hg-contaminated headwater stream.

4. Conclusions and Implications

Mercury isotope ratio measurements spanning three seasonal sampling periods (October, April, and August) suggest a temporal consistency in the sources and biogeochemical transformations influencing the suspended phase along the flow path of EFPC. Changes in both Δ^{199}Hg and δ^{202}Hg values associated with THg_p along the flow path likely resulted from a combination of photochemical reduction (~20%) and microbial reduction (~80%), but may also be partly influenced by the contribution of streambank soils to the streambed. The isotopic composition of the suspended particulate phase was indistinguishable from the biofilm associated with streambed surfaces. Thus, if the predominant location of biogeochemical transformation was within these streambed biofilms, it is not surprising that non-photochemical reduction processes (i.e., microbial reduction) may have been favored. Both suspended particulate and biofilm mercury isotopic composition converged with the isotopic composition of the fine fraction of streambed sediment (<125 μm) along the ~20 km study reach. Overall, these observations suggest that the suspended load isotopic composition during baseflow is altered as it is transported downstream, being repeatedly deposited to, processed within, and re-suspended from the biofilm layer, and progressively mixed with fine sediments along the flow path.

The odd-mass-MIF signature of the dissolved phase was small in magnitude and transient, likely reflecting release of DGM to the water column from photochemical reduction within the suspended particulate phase or streambed biofilm that was subsequently volatilized to the atmosphere. In contrast, the shifts in δ^{202}Hg values of the dissolved phase along the flow path could not be explained by in-stream biogeochemical processes, but rather appeared to be influenced primarily by inputs from the hyporheic zone. Hyporheic exchange appeared to have had the greatest influence on the isotopic composition of dissolved mercury in stream water during August and October when EFPC was less hydrologically connected to the watershed, whereas riparian wetlands appeared to have, at most, a limited influence during April when EFPC was more hydrologically connected to the watershed and the hyporheic zone may have been flushed due to recent high stream flows.

These findings based on mercury isotope systematics contrast in some ways from the conclusions of previous studies of mercury biogeochemistry in EFPC. *Southworth et al.*[15, 16] suggested that ongoing inorganic Hg inputs from Y12 sustain waterborne mercury concentrations during baseflow, whereas particle-bound Hg associated with streambed sediment, biofilm, and streambanks within Lower EFPC are responsible for Hg export during high flow conditions. Mercury isotope analysis suggests that in-stream processing and additional source inputs along Lower EFPC may be more important than originally estimated, even during baseflow. In this study, mercury isotope systematics also suggest that the suspended THg_p load is modified by deposition to, photochemical and microbial reduction within, and resuspension from streambed biofilm during baseflow conditions. It also suggests that the long term mercury

isotopic composition of the fine fraction of streambed sediment likely arises from these processes as well as from possible mixing with streambank soils deposited to the creek. *Southworth et al.*[15] also noted that THg fluxes (not just concentrations) decreased downstream during baseflow conditions, suggesting removal of the suspended load from the water column by the biofilm. Although our study also suggests the importance of streambed biofilm coatings, our THg_p flux estimates increased downstream, further supporting our finding that streambed biofilm was likely a source, as well as a sink, for the suspended load as it spiraled downstream.

We do not know why baseflow total mercury flux (THg = $THg_{(p+d)}$) measurements along EFPC differed between our study and those determined in December 2007.[15] The THg flux across the Y12 boundary (EFK23.4) in 2007 (~ 5 g/d)[15] was similar to the average daily $THg_{(p+d)}$ flux (4.5 ± 0.2 g/d, 1SD) calculated by extrapolating and summing our instantaneous THg_d and THg_p fluxes. However, THg flux at EFK6 in 2007 (~2.6 g/d)[15] was smaller than the average daily $THg_{(p+d)}$ flux (8.1 ± 2.8 g/d, 1SD) we measured downstream at EFK5.0. This implies that conditions along Lower EFPC differed between the two studies. Both studies were sampled under baseflow conditions, although the manual hydrologic discharge measurement associated with sampling was not reported in *Southworth et al,*[15] which makes direct comparisons difficult, and the absence of continuous stream flow monitoring in Lower EFPC in 2007 makes it impossible to assess antecedent flow conditions. Nonetheless, THg flux is typically dominated by the particulate phase, and thus the total suspended solids (TSS) flux may provide some additional insight. The TSS flux across the Y12 boundary in 2007 (~ 60 kg/d) was similar to the 76 ± 17 kg/d (1SD) TSS flux we observed in our study. However, the TSS flux at EFK5.0 in our study ranged from 140 kg/d in October, to 512 kg/d in August, and 687 kg/d in April, which were higher than the ~95 kg/d TSS flux measured during December 2007, and this increased suspended particulate load was likely responsible for observed increases in $THg_{(p+d)}$ flux during our study. Although our study suggests that biofilm dynamics and antecedent flow conditions may be important determinants of the flux of THg_p from Lower EFPC under baseflow conditions, additional studies will be required to determine the precise factors that control whether Lower EFPC acts as a *net* sink or *net* source of THg_p along the flow path at baseflow.

Mercury isotopic measurements suggest that stream water dissolved total mercury concentrations are not entirely sustained by export from Y12 during baseflow, but are augmented primarily by hyporheic exchange and possibly, to a much lesser extent, inputs from riparian wetlands, depending on seasonal hydrologic connectivity and antecedent flow conditions. *Southworth et al.*[15] suggested that mercury associated with streambed sediment and floodplain soils is in highly insoluble fractions, and thus the ongoing dissolved inorganic Hg loading from Y12 should be the predominant source of bioavailable Hg that is methylated within the Lower EFPC ecosystem. However, mercury isotope systematics revealed that the hyporheic zone (and to a much lesser extent, riparian wetlands) may also contribute to dissolved mercury loads in Lower EFPC. Given that the hyporheic zone and riparian wetlands are potentially anoxic sites that can support high rates of MeHg production (e.g., pore waters ranged up to 8.5% of THg as MeHg in the hyporheic zone, and up to 71% of THg as MeHg in riparian wetlands during this

study) (Table S6), the mercury isotopic assessment in this study suggests that the decoupling of inorganic mercury and MeHg in Lower EFPC could, in part, be derived from these legacy sources. $MeHg_d$ concentrations in the hyporheic zone, riparian pore water, and ephemeral riparian tributary surface water were sufficiently elevated to contribute to increases in $MeHg_d$ concentrations in stream water along the flow path (Table S3, Table S6). This somewhat contrasts with recent findings by *Riscassi et al.*[25] that suggested $MeHg_d$ was more likely derived from streambed periphyton rather than diffusive inputs from the hyporheic zone. However, these two hypotheses are not all that inconsistent, as both implicate the streambed as a source of $MeHg_d$ to the water column. Future research should focus on better refining flux estimates along the EFPC corridor, further quantifying the influence of hyporheic exchange and riparian wetlands, identifying the processes that lead to the release of these legacy sources to the water column, and assessing the sources of mercury that are methylated and accumulated within biota.

This research demonstrates that mercury isotopic signatures, imparted by molecular-scale reactions, can be used to gain new insights into process-level controls on the *in-situ* cycling of mercury in complex aquatic ecosystems, and to reveal the sources of legacy mercury contributing to stream water mercury concentrations. As methods for mercury isotopic analysis continue to be refined, it should become possible to also use mercury isotope techniques to assess the influence of non-point-source derived legacy mercury in ecosystems with background concentrations of mercury in soil and water that can result in the bioaccumulation of mercury to levels that are harmful to fish and wildlife. Importantly, this study suggests that different reservoirs of legacy mercury in the environment likely have isotopic signatures that can be differentiated, and thus it should also be possible to track MeHg generated from these various sources into biota. More broadly, this research emphasizes that, similar to non-point-source contaminated ecosystems, mercury mobilization and transport in this highly contaminated headwater stream are strongly influenced by dissolved organic carbon dynamics and hydrological processes. By linking Hg isotopes and hydrology, this study provides a framework for integrating stable Hg isotope techniques with more traditional stream- and watershed-scale approaches and thus may serve as a model for future study of both point-source and non-point-source Hg-contaminated watersheds.

Conflicts of Interest

There are no conflicts of interest to declare.

Acknowledgements

We thank Balaji Anandha Rao and David Kocman for their assistance with field sampling, and Xiangping Yin for DOC, UV absorbance, anion, and MeHg analyses. Sarah North, Emily Seeley, and Renee Veresh provided assistance with preparation of field equipment and sample preparation for isotopic analysis. We thank Marcus Johnson for expert assistance with the operation of the Nu Instruments MC-ICP-MS. This manuscript was improved substantially thanks to the thoughtful comments of Jan Wiederhold and two anonymous reviewers. This

research was supported by the U.S. Department of Energy, Office of Science, Biological and Environmental Research (BER), Subsurface Biogeochemical Research Program under Grant No. DE-SC0007042 and is also a product of the Science Focus Area (SFA) at Oak Ridge National Laboratory (ORNL). ORNL is managed by UT-Batelle LLC for the DOE under Contract No. DE-AC05-000R22725.

References

1 J. P. Hurley, J. M. Benoit, C. L. Babiarz, M. M. Shafer, A. W. Andren, J. R. Sullivan, R. Hammond and D. A. Webb, Influences of watershed characteristics on mercury levels in Wisconsin rivers, *Environ. Sci. Technol.*, 1995, **29**, 1867-1875.

2 C. J. Oswald, A. Heyes and B. A. Branfireun, Fate and transport of ambient mercury and applied mercury isotope in terrestrial upland soils: Insights from the METAALICUS watershed, *Environ. Sci. Technol.*, 2014, **48**, 1023-1031.

3 H. Hintelmann, R. Harris, A. Heyes, J. P. Hurley, C. A. Kelly, D. P. Krabbenhoft, S. Lindberg, J. W. M. Rudd, K. J. Scott and V. L. St Louis, Reactivity and mobility of new and old mercury deposition in a boreal forest ecosystem during the first year of the METAALICUS study, *Environ. Sci. Technol.*, 2002, **36**, 5034-5040.

4 D. A. Burns, K. Riva-Murray, P. M. Bradley, G. R. Aiken and M. E. Brigham, Landscape controls on total and methyl Hg in the upper Hudson River basin, New York, USA, *J. Geophys. Res.-Biogeosciences*, 2012, **117**,

5 V. L. St. Louis, J. W. M. Rudd, C. A. Kelly, K. G. Beaty, R. J. Flett and N. T. Roulet, Production and loss of methylmercury and loss of total mercury from boreal forest catchments containing different types of wetlands, *Environmental Science & Technology*, 1996, **30**, 2719-2729.

6 J. B. Shanley, N. C. Kamman, T. A. Clair and A. Chalmers, Physical controls on total and methylmercury concentrations in streams and lakes of the northeastern USA, *Ecotoxicology*, 2005, **14**, 125-134.

7 J. B. Shanley, M. A. Mast, D. H. Campbell, G. R. Aiken, D. P. Krabbenhoft, R. J. Hunt, J. F. Walker, P. F. Schuster, A. Chalmers, B. T. Aulenbach, N. E. Peters, M. Marvin-DiPasquale, D. W. Clow and M. M. Shafer, Comparison of total mercury and methylmercury cycling at five sites using the small watershed approach, *Environ. Pollut.*, 2008, **154**, 143-154.

8 J. A. Dittman, J. B. Shanley, C. T. Driscoll, G. R. Aiken, A. T. Chalmers, J. E. Towse and P. Selvendiran, Mercury dynamics in relation to dissolved organic carbon concentration and quality during high flow events in three northeastern US streams, *Water. Resour. Res.*, 2010, **46**,

9 J. Schelker, D. A. Burns, M. Weiler and H. Laudon, Hydrological mobilization of mercury and dissolved organic carbon in a snow-dominated, forested watershed: Conceptualization and modeling, *J. Geophys. Res.-Biogeosciences*, 2011, **116**,

10 T. Scherbatskoy, J. B. Shanley and G. J. Keeler, Factors controlling mercury transport in an upland forested catchment, *Water Air Soil Poll.*, 1998, **105**, 427-438.

11 A. L. Riscassi and T. M. Scanlon, Controls on stream water dissolved mercury in three mid-Appalachian forested headwater catchments, *Water. Resour. Res.*, 2011, **47**,

12 H. Hintelmann, Use of stable isotopes in mercury research, *in* Mercury in the environment: Pattern and process, M. S. Bank, University of California Press, Berkeley, 2012, 55-71.

13 J. D. Blum, L. S. Sherman and M. W. Johnson, Mercury isotopes in earth and environmental sciences, *Annu. Rev. Earth Pl. Sc.*, 2014, **42**, 249-269.
14 S. C. Brooks and G. R. Southworth, History of mercury use and environmental contamination at the Oak Ridge Y-12 Plant, *Environ. Pollut.*, 2011, **159**, 219-228.
15 G. Southworth, T. Mathews, M. Greeley, M. Peterson, S. Brooks and D. Ketelle, Sources of mercury in a contaminated stream-implications for the timescale of recovery, *Environ. Toxicol. Chem.*, 2013, **32**, 764-772.
16 G. Southworth, M. Greeley, M. Peterson, K. Lowe and R. Ketelle, Sources of mercury to East Fork Poplar Creek downstream from the Y-12 National Security Complex: Inventories and export rates, ORNL/TM-2009/231. Oak Ridge National Laboratory, Oak Ridge, TN., 2010.
17 M. Amyot, G. Southworth, S. E. Lindberg, H. Hintelmann, J. D. Lalonde, N. Ogrinc, A. J. Poulain and K. A. Sandilands, Formation and evasion of dissolved gaseous mercury in large enclosures amended with $(HgCl_2)$-^{200}Hg, *Atmos. Environ.*, 2004, **38**, 4279-4289.
18 A. J. Poulain, D. M. Orihel, M. Amyot, M. J. Paterson, H. Hintelmann and G. R. Southworth, Relationship to aquatic between the loading rate of inorganic mercury ecosystems and dissolved gaseous mercury production and evasion, *Chemosphere*, 2006, **65**, 2199-2207.
19 A. J. Poulain, M. Amyot, D. Findlay, S. Telor, T. Barkay and H. Hintelmann, Biological and photochemical production of dissolved gaseous mercury in a boreal lake, *Limnol. Oceanogr.*, 2004, **49**, 2265-2275.
20 G. Southworth, S. Lindberg, H. Hintelmann, M. Amyot, A. Poulain, M. Bogle, M. Peterson, J. Rudd, R. Harris, K. Sandilands, D. Krabbenhoft and M. Olsen, Evasion of added isotopic mercury from a northern temperate lake, *Environ. Toxicol. Chem.*, 2007, **26**, 53-60.
21 W. M. Dong, L. Y. Liang, S. Brooks, G. Southworth and B. H. Gu, Roles of dissolved organic matter in the speciation of mercury and methylmercury in a contaminated ecosystem in Oak Ridge, Tennessee, *Environ. Chem.*, 2009, **7**, 94-102.
22 B. Gu, B. Mishra, C. Miller, W. Wang, B. Lai, S. C. Brooks, K. M. Kemner and L. Liang, X-ray fluorescence mapping of mercury on suspended mineral particles and diatoms in a contaminated freshwater system, *Biogeosciences*, 2014, **11**, 5259-5267.
23 C. L. Miller, G. Southworth, S. Brooks, L. Liang and B. Gu, Kinetic controls on the complexation between mercury and dissolved organic matter in a contaminated environment, *Environ. Sci. Technol.*, 2009, **43**, 8548-8553.
24 J. M. Loar, A. J. Stewart and J. G. Smith, Twenty-five years of ecological recovery of East Fork Poplar Creek: Review of environmental problems and remedial actions, *Environ. Manage.*, 2011, **47**, 1010-1020.
25 A. Riscassi, C. Miller and S. Brooks, Seasonal and flow-driven dynamics of particulate and dissolved mercury and methylmercury in a stream impacted by an industrial mercury source, *Environ. Toxicol. Chem.*, 2016, **35**, 1386-1400.
26 M. O. Barnett, L. A. Harris, R. R. Turner, T. J. Henson, R. E. Melton and R. J. Stevenson, Characterization of mercury species in contaminated floodplain soils, *Water Air Soil Poll.*, 1995, **80**, 1105-1108.
27 M. O. Barnett, L. A. Harris, R. R. Turner, R. J. Stevenson, T. J. Henson, R. C. Melton and D. P. Hoffman, Formation of mercuric sulfide in soil, *Environ. Sci. Technol.*, 1997, **31**, 3037-3043.
28 M. O. Barnett and R. R. Turner, Bioaccessibility of mercury in soils, *Soil & Sediment Contamination*, 2001, **10**, 301-316.

29 C. L. Miller, D. B. Watson, B. P. Lester, K. A. Lowe, E. M. Pierce and L. Liang, Characterization of soils from an industrial complex contaminated with elemental mercury, *Environ. Res.*, 2013, **125**, 20-29.

30 B. A. Poulin, G. R. Aiken, K. L. Nagy, A. Monceau, D. P. Krabbenhoft and J. N. Ryan, Mercury transformation and release differs with depth and time in a contaminated riparian soil during simulated flooding, *Geochim. Cosmochim. Acta*, 2016, **176**, 118-138.

31 G. R. Southworth, R. R. Turner, M. J. Peterson, M. A. Bogle and M. G. Ryon, Response of mercury contamination in fish to decreased aqueous concentrations and loading of inorganic mercury in a small stream, *Environ. Monit. Assess.*, 2000, **63**, 481-494.

32 T. E. Widner, T. R. Mongan, G. M. Bruce and S. M. Flack, Reports of the Oak Ridge dose reconstruction, volume 2: Mercury releases from lithium enrichment at the Oak Ridge Y-12 plant - A reconstruction of historical releases and off-site doses and health risks. Submitted to theTennessee Department of Health by ChemRisk: A Service of McLaren/Hart, Alameda, CA, 1999.

33 T. E. Widner, T. R. Mongan, G. M. Bruce and S. M. Flack, Reports of the Oak Ridge dose reconstruction, volume 2a: Mercury releases from lithium enrichment at the Oak Ridge Y-12 plant - A reconstruction of historical releases and off-site doses and health risks - Appendices, submitted to theTennessee Department of Health by ChemRisk: A service of McLaren/Hart. Alameda, CA, 1999.

34 P. M. Donovan, J. D. Blum, J. D. Demers, B. Gu, S. C. Brooks and J. Peryam, Identification of multiple mercury sources to stream sediments near Oak Ridge, TN, USA, *Environ. Sci. Technol.*, 2014, **48**, 3666-3674.

35 J. D. Demers, C. T. Driscoll and J. B. Shanley, Mercury mobilization and episodic stream acidification during snowmelt: Role of hydrologic flow paths, source areas, and supply of dissolved organic carbon, *Water. Resour. Res.*, 2010, **46**,

36 D. F. Flohr, J. W. Garrett, J. T. Hamilton and T. D. Phillips, Water resources data, Tennessee water year 2002: TN-02-1, 2002, 442.

37 J. F. Lowery, P. H. Counts, F. D. Edwards and J. W. Garrett, Water resources data, Tennessee, water year 1988: TN-88-1, 1988, 442.

38 J. R. Taylor, An Introduction to Error Analysis: The Study of Uncertainties in Physical Measurements, 2nd Edition, University Science Books, Sausalito, CA, 1997, 327 pp.

39 USEPA, Method 1631: Measurement of mercury in water; Revision E. U.S. Environmental Protection Agency, Office of Water, Office of Science and Technology, Engineering and Analysis Division (4303), Washington, D.C., USA, 1998.

40 USEPA, Method 1630: Methyl mercury in water by distillation, aqueous ethylation, purge and trap, and cold vapor atomic fluorescence spectrometry. U.S. Environmental Protection Agency, Office of Water, Office of Science and Technology, Engineering and Analysis Division (4303), Washington D.C., 2001.

41 H. Hintelmann and N. Ogrinc, Determination of stable mercury isotopes by ICP/MS and their application in environmental studies, *in* Biogeochemistry of Environmentally Important Trace Elements, 2003, 321-338.

42 J. L. Weishaar, G. R. Aiken, B. A. Bergamaschi, M. S. Fram, R. Fujii and K. Mopper, Evaluation of specific ultraviolet absorbance as an indicator of the chemical composition and reactivity of dissolved organic carbon, *Environ. Sci. Technol.*, 2003, **37**, 4702-4708.

43 Y. Qian, X. Yin, H. Lin, B. Rao, S. C. Brooks, L. Liang and B. Gu, Why dissolved organic matter enhances photodegradation of methylmercury, *Environ. Sci. Technol. Letters*, 2014, **1**, 426-431.
44 H. Hu, H. Lin, W. Zheng, S. J. Tomanicek, A. Johs, X. Feng, D. A. Elias, L. Liang and B. Gu, Oxidation and methylation of dissolved elemental mercury by anaerobic bacteria, *Nature Geosci.*, 2013, **6**, 751-754.
45 J. D. Demers, J. D. Blum and D. R. Zak, Mercury isotopes in a forested ecosystem: Implications for air-surface exchange dynamics and the global mercury cycle, *Global Biogeochem. Cycles*, 2013, **27**, 222-238.
46 D. S. Lauretta, B. Klaue, J. D. Blum and P. R. Buseck, Mercury abundances and isotopic compositions in the Murchison (CM) and Allende (CV) carbonaceous chondrites, *Geochim. Cosmochim. Acta*, 2001, **65**, 2807-2818.
47 J. D. Blum and B. A. Bergquist, Reporting of variations in the natural isotopic composition of mercury, *Anal. Bioanal. Chem.*, 2007, **388**, 353-359.
48 G. R. Southworth, M. J. Peterson and M. A. Bogle, Bioaccumulation factors for mercury in stream fish, *Environmental Practice*, 2004, **6**, 135-143.
49 S. Brooks, V. Eller, J. Dickson, J. Earles, K. Lowe, T. Mehlhorn, T. Olsen, C. DeRolph, D. Watson, D. Phillips and M. Peterson, Mercury Content of Sediments in East Fork Poplar Creek: Current Assessment and Past Trends, ORNL/TM-2016/578. Oak Ridge National Laboratory, Oak Rdige, TN, 2017.
50 D. Watson, S. Brooks, T. Mathews, M. Bevelhimer, C. DeRolph, C. Brandt, M. Peterson and R. Ketelle, Evaluation of Lower East Fork Poplar Creek Mercury Sources, ORNL/TM-2016/134. Oak Ridge National Laboratory, Oak Ridge, TN, 2016.
51 P. M. Bradley, C. A. Journey, M. E. Brigham, D. A. Burns, D. T. Button and K. Riva-Murray, Intra- and inter-basin mercury comparisons: Importance of basin scale and time-weighted methylmercury estimates, *Environ. Pollut.*, 2013, **172**, 42-52.
52 V. L. St. Louis, J. W. M. Rudd, C. A. Kelly, K. G. Beaty, N. S. Bloom and R. J. Flett, Importance of wetlands as sources of methyl mercury to boreal forest ecosystems, *Can. J. Fish Aquat. Sci.*, 1994, **51**, 1065-1076.
53 K. Bishop, Y. H. Lee, C. Pettersson and B. Allard, Terrestrial sources of methylmercury in surface waters - The Importance of the riparian zone on the Svartberget catchment, *Water Air Soil Poll.*, 1995, **80**, 435-444.
54 R. Sun, D. G. Streets, H. M. Horowitz, H. M. Amos, G. Liu, V. Perrot, J. P. Toutain, H. Hintelmann, E. M. Sunderland and J. E. Sonke, Historical (1850-2010) mercury stable isotope inventory from anthropogenic sources to teh atmosphere., *Elementa: Science of the Anthropocene*, 2016,
55 W. Zheng and H. Hintelmann, Isotope fractionation of mercury during its photochemical reduction by low-molecular-weight organic compounds, *J. Phys. Chem. A.*, 2010, **114**, 4246-4253.
56 J. D. Newbold, J. W. Elwood, R. V. Oneill and W. Vanwinkle, Measuring nutrient spiralling in streams, *Can. J. Fish Aquat. Sci.*, 1981, **38**, 860-863.
57 B. Gu, Y. Bian, C. L. Miller, W. Dong, X. Jiang and L. Liang, Mercury reduction and complexation by natural organic matter in anoxic environments, *P. Natl. Acad. Sci. USA*, 2011, **108**, 1479-1483.
58 F. He, W. Zhao, L. Liang and B. Gu, Photochemical oxidation of dissolved elemental mercury by carbonate radicals in water, *Environ. Sci. Technol. Letters*, 2014, **1**, 499-503.

59 F. He, W. Zheng, L. Liang and B. Gu, Mercury photolytic transformation affected by low-molecular-weight natural organics in water, *Sci Total Environ.*, 2012, **416**, 429-435.
60 W. Zheng, L. Liang and B. Gu, Mercury reduction and oxidation by reduced natural organic matter in anoxic environments, *Environ. Sci. Technol.*, 2012, **46**, 292-299.
61 A. Manceau, C. Lemouchi, M. Enescu, A.-C. Gaillot, M. Lanson, V. Magnin, P. Glatzel, B. A. Poulin, J. N. Ryan, G. R. Aiken, I. Gautier-Luneau and K. L. Nagy, Formation of mercury sulfide from Hg(II)-thiolate complexes in natural organic matter, *Environ. Sci. Technol.*, 2015, **49**, 9787-9796.
62 W. Dong, Y. Bian, L. Liang and B. Gu, Binding constants of mercury and dissolved organic matter determined by a modified ion exchange technique, *Environ. Sci. Technol.*, 2011, **45**, 3576-3583.
63 P. Rodriguez-Gonzalez, V. N. Epov, R. Bridou, E. Tessier, R. Guyoneaud, M. Monperrus and D. Amouroux, Species-specific stable isotope fractionation of mercury during Hg(II) methylation by an anaerobic bacteria (Desulfobulbus propionicus) under dark conditions, *Environ. Sci. Technol.*, 2009, **43**, 9183-9188.
64 W. Zheng and H. Hintelmann, Nuclear field shift effect in isotope fractionation of mercury during abiotic reduction in the absence of light, *J. Phys. Chem. A.*, 2010, **114**, 4238-4245.
65 K. Kritee, J. D. Blum and T. Barkay, Mercury stable isotope fractionation during reduction of Hg(II) by different microbial pathways, *Environ. Sci. Technol.*, 2008, **42**, 9171-9177.
66 K. Kritee, T. Barkay and J. D. Blum, Mass dependent stable isotope fractionation of mercury during mer mediated microbial degradation of monomethylmercury, *Geochim. Cosmochim. Acta*, 2009, **73**, 1285-1296.
67 B. A. Bergquist and J. D. Blum, Mass-dependent and -independent fractionation of Hg isotopes by photoreduction in aquatic systems, *Science*, 2007, **318**, 417-420.
68 W. Zheng and H. Hintelmann, Mercury isotope fractionation during photoreduction in natural water is controlled by its Hg/DOC ratio, *Geochim. Cosmochim. Acta*, 2009, **73**, 6704-6715.
69 K. Kritee, J. D. Blum, M. W. Johnson, B. A. Bergquist and T. Barkay, Mercury stable isotope fractionation during reduction of Hg(II) to Hg(0) by mercury resistant microorganisms, *Environ. Sci. Technol.*, 2007, **41**, 1889-1895.
70 H. Hu, H. Lin, W. Zheng, B. Rao, X. Feng, L. Liang, D. A. Elias and B. Gu, Mercury reduction and cell-surface adsorption by geobacter sulfurreducens PCA, *Environ. Sci. Technol.*, 2013, **47**, 10922-10930.
71 A. J. Poulain, S. M. N. Chadhain, P. A. Ariya, M. Amyot, E. Garcia, P. G. C. Campbell, G. J. Zylstra and T. Barkay, Potential for mercury reduction by microbes in the high arctic, *Appl. Environ. Microb.*, 2007, **73**, 2230-2238.
72 T. Barkay, S. M. Miller and A. O. Summers, Bacterial mercury resistance from atoms to ecosystems, *Fems Microbiol. Rev.*, 2003, **27**, 355-384.
73 D. Foucher, H. Hintelmann, T. A. Al and K. T. MacQuarrie, Mercury isotope fractionation in waters and sediments of the Murray Brook mine watershed (New Brunswick, Canada): Tracing mercury contamination and transformation, *Chem. Geol.*, 2013, **336**, 87-95.
74 R. S. Smith, J. G. Wiederhold and R. Kretzschmar, Mercury isotope fractionation during precipitation of metacinnabar (beta-HgS) and montroydite (HgO), *Environ. Sci. Technol.*, 2015, **49**, 4325-4334.

75 J. G. Wiederhold, C. J. Cramer, K. Daniel, I. Infante, B. Bourdon and R. Kretzschmar, Equilibrium mercury isotope fractionation between dissolved Hg(II) species and thiol-bound Hg, *Environ. Sci. Technol.*, 2010, **44**, 4191-4197.

76 M. Jiskra, J. G. Wiederhold, B. Bourdon and R. Kretzschmar, Solution speciation controls mercury isotope fractionation of Hg(II) sorption to goethite, *Environ. Sci. Technol.*, 2012, **46**, 6654-6662.

77 M. Jiskra, D. Saile, J. G. Wiederhold, B. Bourdon, E. Bjorn and R. Kretzschmar, Kinetics of Hg(II) exchange between organic ligands, goethite, and natural organic matter studied with an enriched stable isotope approach, *Environ. Sci. Technol.*, 2014, **48**, 13207-13217.

78 S. J. Washburn, J. D. Blum, J. D. Demers, A. Y. Kurz and R. C. Landis, Isotopic characterization of mercury downstream of historic industrial contamination in the South River, Virginia, *Environ. Sci. Technol.*, 2017, **51**, 10965-10973.

79 J. B. Chen, H. Hintelmann, W. Zheng, X. B. Feng, H. M. Cai, Z. H. Wang, S. L. Yuan and Z. W. Wang, Isotopic evidence for distinct sources of mercury in lake waters and sediments, *Chem. Geol.*, 2016, **426**, 33-44.

80 M. Jiskra, J. G. Wiederhold, U. Skyllberg, R. M. Kronberg and R. Kretzschmar, Source tracing of natural organic matter bound mercury in boreal forest runoff with mercury stable isotopes, *Environmental Science-Processes & Impacts*, 2017, **19**, 1235-1248.

81 L. E. Gratz, G. J. Keeler, J. D. Blum and L. S. Sherman, Isotopic composition and fractionation of mercury in Great Lakes precipitation and ambient air, *Environ. Sci. Technol.*, 2010, **44**, 7764-7770.

82 L. S. Sherman, J. D. Blum, G. J. Keeler, J. D. Demers and J. T. Dvonch, Investigation of local mercury deposition from a coal-fired power plant using mercury isotopes, *Environ. Sci. Technol.*, 2012, **46**, 382-390.

83 J. B. Chen, H. Hintelmann, X. B. Feng and B. Dimock, Unusual fractionation of both odd and even mercury isotopes in precipitation from Peterborough, ON, Canada, *Geochim. Cosmochim. Acta*, 2012, **90**, 33-46.

84 L. S. Sherman, J. D. Blum, J. T. Dvonch, L. E. Gratz and M. S. Landis, The use of Pb, Sr, and Hg isotopes in Great Lakes precipitation as a tool for pollution source attribution, *Sci Total Environ.*, 2015, **502**, 362-374.

85 J. A. Dittman, J. B. Shanley, C. T. Driscoll, G. R. Aiken, A. T. Chalmers and J. E. Towse, Ultraviolet absorbance as a proxy for total dissolved mercury in streams, *Environ. Pollut.*, 2009, **157**, 1953-1956.

Figure Legends

Figure 1. Map of synoptic sampling sites along the flow path of East Fork Poplar Creek (EFPC) in Oak Ridge, TN, USA. Synoptic sampling sites are identified by a three letter code (EFK) corresponding to the stream, followed by the kilometers upstream from its confluence with Poplar Creek. Intensive hyporheic pore water sampling sites were located at EFK5.0 and EFK22.3; Y12-impacted riparian wetland sampling site was located at EFK22.3. The regional reference site for this study (Hinds Creek, HCK10) is located ~25 km northeast of Y12, and is a tributary to the Clinch River (see *Donovan et al.*[34]).

Figure 2. Components of flux of (A) total dissolved mercury (THg_d), and (B) total particulate mercury (THg_p) at EFK5.0 in East Fork Poplar Creek, Oak Ridge, TN, USA. Fluxes of diffuse legacy Hg, Oak Ridge wastewater treatment facility (ORWTF) and tributary Hg, and Y12-contributed Hg are shown relative to total flux at EFK5.0. Flux data (µg/s) are located in Table 1.

Figure 3. Isotopic composition and concentration of particulate-bound mercury (THg_p). Shown are (A) δ^{202}Hg values and (B) Δ^{199}Hg values associated with total suspended solids (n=24), biofilm (n = 6), and the fine fraction of streambed sediment (<125 µm; n = 6), and (C) concentrations of THg_p associated with total suspended solids along the flow path of East Fork Poplar Creek, Oak Ridge, TN, USA. Analytical uncertainty of delta values is shown as 2SD of average of session averages for UM-Almaden (see *Methods*). Regression lines include THg_p data points, but exclude biofilm. Shaded area shows range of (A) δ^{202}Hg values and (B) Δ^{199}Hg values of fine fraction streambed sediments, as previously reported by *Donovan et al.*[34]

Figure 4. Isotopic composition and concentration of dissolved mercury (THg_d). Shown are (A) δ^{202}Hg values (n=23), (B) Δ^{199}Hg values (n=23), and (C) concentrations (n=24) associated with stream water along the flow path of East Fork Poplar Creek, Oak Ridge, TN, USA. Analytical uncertainty is shown as 2SD of average of session averages for UM-Almaden (see *Methods*).

Figure 5. Offset between δ^{202}Hg values of dissolved Hg (THg_d) and particulate-bound Hg (THg_p) associated with total suspended solids along the flow path of East Fork Poplar Creek, Oak Ridge, TN, USA. Gray dashed line shows zero values for $\delta^{202}Hg_{p-d}$.

Figure 6. Mercury isotopic composition (δ^{202}Hg vs Δ^{199}Hg) of dissolved Hg (THg_d) in stream water (n = 23), hyporheic pore water (n = 11), and riparian surface water and pore water (n = 5); and particulate-bound mercury (THg_p) (n = 24) associated with total suspended solids along the flow path of East Fork Poplar Creek, Oak Ridge, TN, USA. Analytical uncertainty is shown as 2SD of average of session averages for UM-Almaden (see *Methods*). Gray dashed lines show zero values for δ^{202}Hg and Δ^{199}Hg.

Figure 7. Relationships among dissolved organic carbon (DOC), specific UV absorbance at 254 nm ($SUVA_{254}$), and distance along the flow path of East Fork Poplar Creek (EFPC) in Oak Ridge, TN, USA. Regression lines are plotted only for statistically significant slope values ($p < 0.05$).

Figure 1. Map of synoptic sampling sites along the flow path of East Fork Poplar Creek (EFPC) in Oak Ridge, TN, USA. Synoptic sampling sites are identified by a three letter code (EFK) corresponding to the stream, followed by the kilometers upstream from its confluence with Poplar Creek. Intensive hyporheic pore water sampling sites were located at EFK5.0 and EFK22.3; Y12-impacted riparian wetland sampling site was located at EFK22.3. The regional reference site for this study (Hinds Creek, HCK10) is located ~25 km northeast of Y12, and is a tributary to the Clinch River (see *Donovan et al.*[34]).

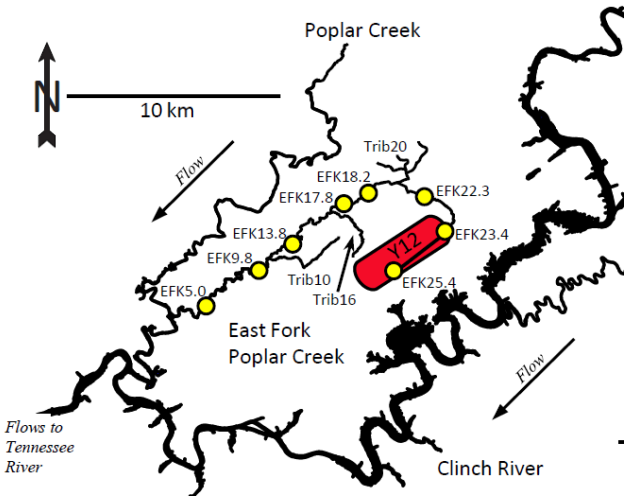

Figure 2. Components of flux of (A) total dissolved mercury (THg_d), and (B) total particulate mercury (THg_p) at EFK5.0 in East Fork Poplar Creek, Oak Ridge, TN, USA. Fluxes of diffuse legacy Hg, Oak Ridge wastewater treatment facility (ORWTF) and tributary Hg, and Y12-contributed Hg are shown relative to total flux at EFK5.0. Flux data (µg/s) are located in Table 1.

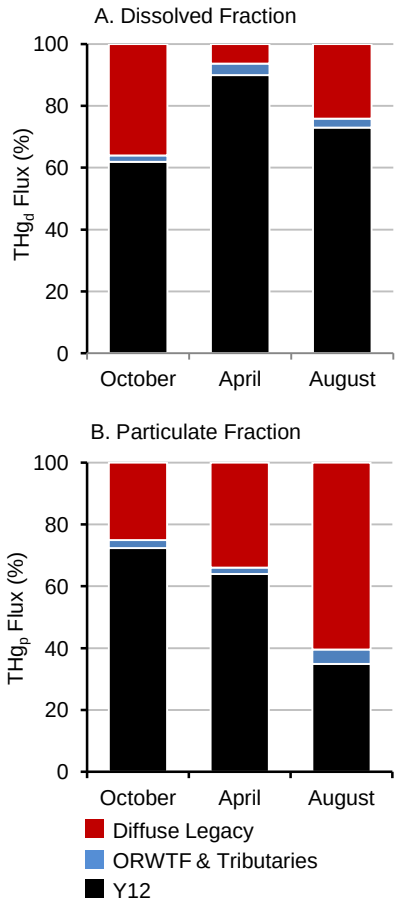

Figure 3. Isotopic composition and concentration of particulate-bound mercury (THg_p). Shown are (A) $\delta^{202}Hg$ values and (B) $\Delta^{199}Hg$ values associated with total suspended solids (n=24), biofilm (n = 6), and the fine fraction of streambed sediment (<125 µm; n = 6), and (C) concentrations of THg_p associated with total suspended solids along the flow path of East Fork Poplar Creek, Oak Ridge, TN, USA. Analytical uncertainty of delta values is shown as 2SD of average of session averages for UM-Almaden (see *Methods*). Regression lines include THg_p data points, but exclude biofilm. Shaded area shows range of (A) $\delta^{202}Hg$ values and (B) $\Delta^{199}Hg$ values of fine fraction streambed sediments, as previously reported by *Donovan et al.*[34]

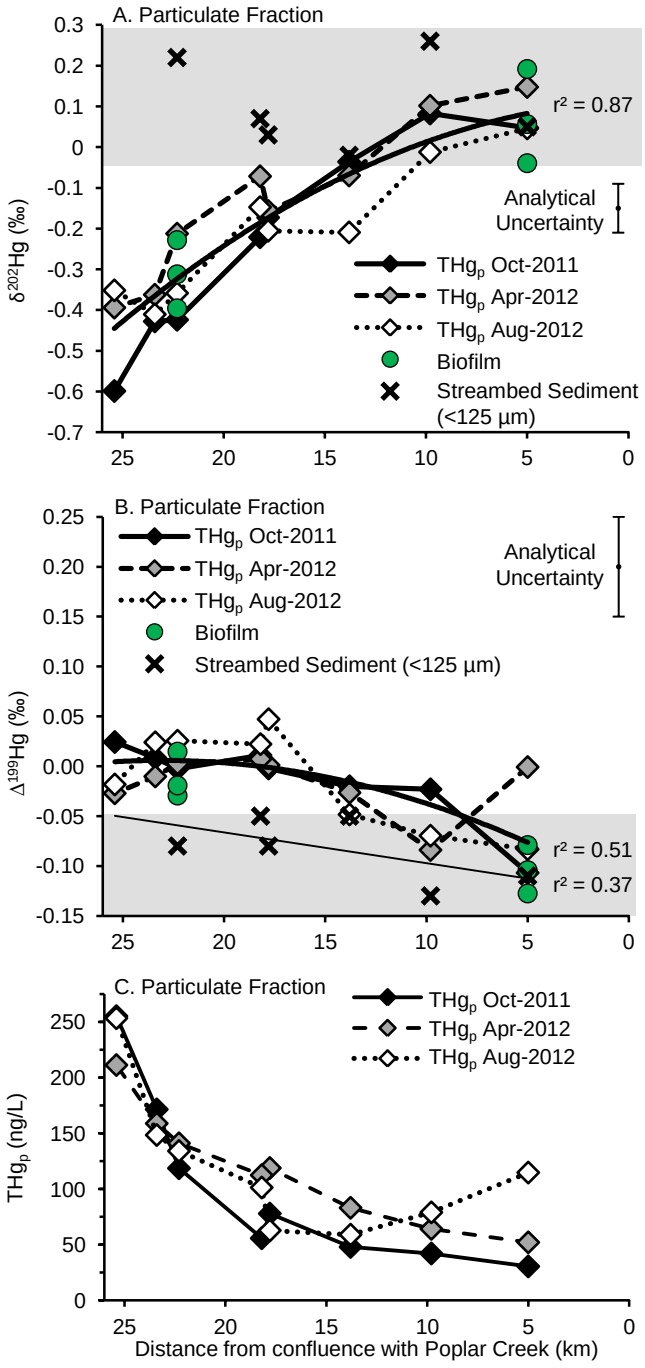

Figure 4. Isotopic composition and concentration of dissolved mercury (THg_d). Shown are (A) $\delta^{202}Hg$ values (n=23), (B) $\Delta^{199}Hg$ values (n=23), and (C) concentrations (n=24) associated with stream water along the flow path of East Fork Poplar Creek, Oak Ridge, TN, USA. Analytical uncertainty is shown as 2SD of average of session averages for UM-Almaden (see *Methods*).

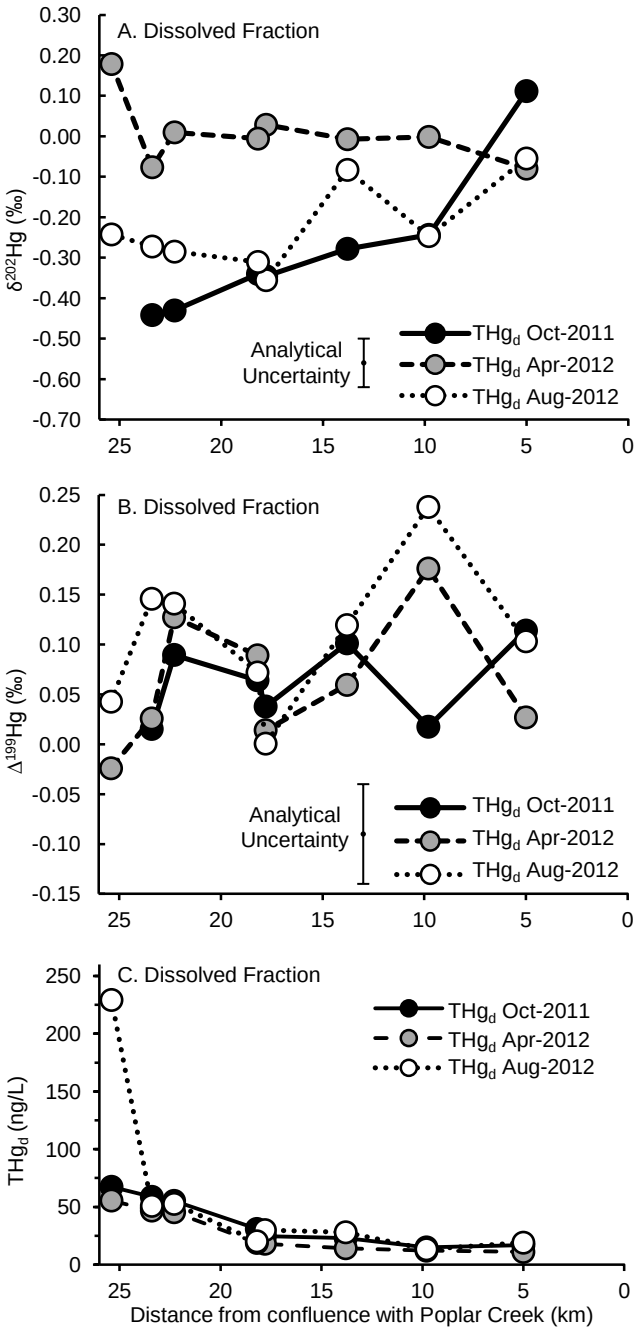

Figure 5. Offset between $\delta^{202}Hg$ values of dissolved Hg (THg_d) and particulate-bound Hg (THg_p) associated with total suspended solids along the flow path of East Fork Poplar Creek, Oak Ridge, TN, USA. Gray dashed line shows zero values for $\delta^{202}Hg_{p-d}$.

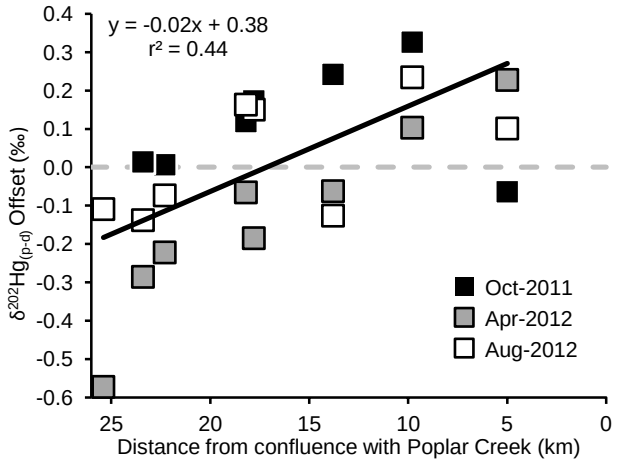

Figure 6. Mercury isotopic composition (δ^{202}Hg vs. Δ^{199}Hg) of dissolved Hg (THg_d) in stream water (n = 23), hyporheic porewater (n = 11), and riparian surface water and porewater (n = 5); and particulate-bound mercury (THg_p) (n = 24) associated with total suspended solids along the flow path of East Fork Poplar Creek, Oak Ridge, TN, USA. Analytical uncertainty is shown as 2SD of average of session averages for UM-Almaden (see *Methods*). Gray dashed lines show zero values for δ^{202}Hg and Δ^{199}Hg.

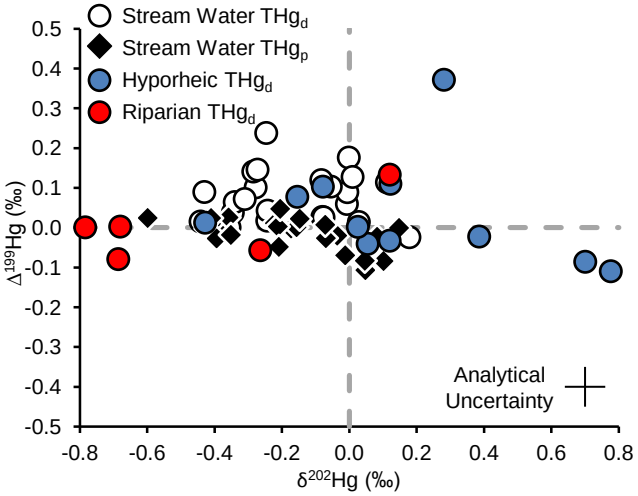

Figure 7. Relationships among dissolved organic carbon (DOC), specific UV absorbance at 254 nm ($SUVA_{254}$), and distance along the flow path of East Fork Poplar Creek (EFPC) in Oak Ridge, TN, USA. Regression lines are plotted only for statistically significant slope values ($p < 0.05$).

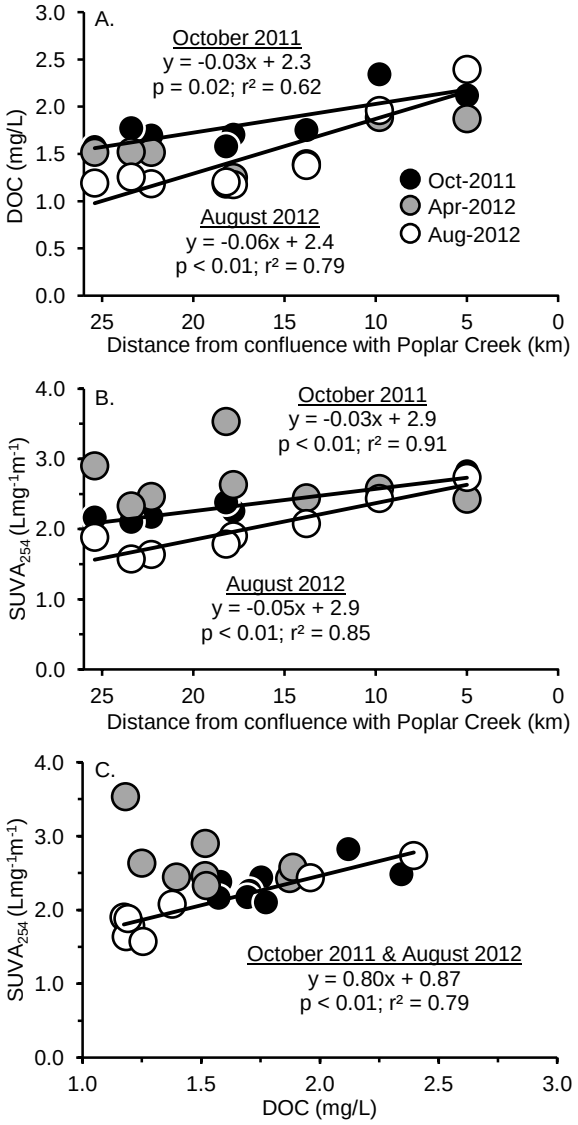

Table 1. Stream water discharge (m^3/s), and flux of total dissolved mercury (THg_d) and particulate-bound mercury (THg_p) from EFK23.4, the Oak Ridge wastewater treatment facility (ORWTF) that discharges at EFK13.5, tributaries and diffuse sources upstream of EFK5.0, and EFK5.0 in East Fork Poplar Creek, Oak Ridge, TN, USA.[a]

	Discharge (m^3/s)			
	EFK23.4	ORWTF	Tributaries & Diffuse	EFK5.0
October	0.24 ± 0.02	0.12 ± 0.01	0.59 ± 0.10	0.95 ± 0.10
April	0.26 ± 0.03	0.13 ± 0.01	0.84 ± 0.13	1.22 ± 0.12
August	0.26 ± 0.03	0.14 ± 0.01	0.57 ± 0.10	0.97 ± 0.10

	THg_d Flux (µg/s)				
	EFK23.4	ORWTF	Tributaries	Diffuse	EFK5.0
October	11.5 ± 1.5	0.201 ± 0.026	0.169 ± 0.032	6.70 ± 2.86	18.6 ± 2.4
April	12.5 ± 1.6	0.443 ± 0.058	0.085 ± 0.015	0.88 ± 2.45	13.9 ± 1.8
August	13.9 ± 1.8	0.211 ± 0.028	0.329 ± 0.065	4.60 ± 3.08	19.0 ± 2.5

	THg_p Flux (µg/s)				
	EFK23.4	ORWTF	Tributaries	Diffuse	EFK5.0
October	38.2 ± 5.0	0.309 ± 0.040	1.03 ± 0.20	13.2 ± 8.5	52.7 ± 6.9
April	40.8 ± 5.3	0.200 ± 0.026	1.09 ± 0.19	21.6 ± 9.9	63.8 ± 8.3
August	38.9 ± 5.1	0.228 ± 0.030	4.94 ± 0.98	67.5 ± 15.5	111 ± 14.6

[a]Discharge and flux calculations are detailed in methods, uncertainties are based on propagation of error associated with discharge and concentration data, and are likely ≥ 1SD (*see* section 2.3). Location of EFK23.4 and EFK5.0 are shown on site map (Figure 1).

Table 2. Mercury isotopic composition of UM-Almaden and procedural standards.[a]

Standard Type	*n*	δ^{204}Hg (‰)	2σ (‰)	δ^{202}Hg (‰)	2σ (‰)	δ^{201}Hg (‰)	2σ (‰)	δ^{200}Hg (‰)	2σ (‰)	δ^{199}Hg (‰)	2σ (‰)	Δ^{204}Hg (‰)	2σ (‰)	Δ^{201}Hg (‰)	2σ (‰)	Δ^{200}Hg (‰)	2σ (‰)	Δ^{199}Hg (‰)	2σ (‰)
UM-Almaden	34	-0.88	0.09	-0.58	0.06	-0.48	0.05	-0.27	0.06	-0.16	0.06	-0.02	0.11	-0.04	0.04	0.02	0.04	-0.02	0.05
Purge & Trap (NIST SRM 3133)	14	0.03	0.05	0.04	0.04	0.01	0.03	0.04	0.04	0.04	0.02	-0.03	0.05	-0.02	0.02	0.03	0.03	0.03	0.02
Apple Leaves (NIST SRM 1515)	5	-3.89	0.07	-2.65	0.03	-2.03	0.04	-1.37	0.02	-0.63	0.04	0.07	0.05	-0.04	0.03	-0.04	0.02	0.04	0.03
NY/NJ Waterway Sediment (NIST SRM 1944)	8	-0.68	0.06	-0.46	0.03	-0.37	0.02	-0.23	0.02	-0.12	0.03	0.01	0.02	-0.03	0.01	0.00	0.02	-0.01	0.03

[a]For UM-Almaden, *n* is the number of preparations (i.e., the number of session averages, with separate values for preparations at different concentrations within a session). For procedural standards, *n* is the number of completely independent preparations of the material. The 2σ for UM-Almaden shows 2SD of the average of session averages; whereas the 2σ for purge & trap standards and reference materials show 2SE of the average of session averages (see *Methods*).